

Natural Abundance ^{14}N and ^{15}N Solid-State NMR of Pharmaceuticals and their Polymorphs

Stanislav L. Veinberg,¹ Karen E. Johnston,² Michael J. Jaroszewicz,¹ Brianna M. Kispal,¹
Christopher R. Mireault,¹ Takeshi Kobayashi,³ Marek Pruski^{3,4,*} and Robert W. Schurko^{1,*}

¹Department of Chemistry and Biochemistry, University of Windsor, Windsor, Ontario, N9B
3P4, Canada

²Department of Chemistry, Durham University, Durham, DH1 3L3, United Kingdom

³U.S. DOE Ames Laboratory, Iowa State University, Ames, Iowa, 50011-3020, USA

⁴Department of Chemistry, Iowa State University, Ames, IA 50011-3020, USA

*Authors to whom correspondence should be addressed

R.W. Schurko, Phone: (519) 253-3000 x3548, Fax: (519) 973-7098;

Electronic mail: rschurko@uwindsor.ca

M. Pruski, Phone: (515) 294-2017, Fax (515) 294-4709;

Electronic mail: mpruski@iastate.edu

Abstract

^{14}N ultra-wideline (UW), $^1\text{H}\{^{15}\text{N}\}$ indirectly-detected HETCOR (idHETCOR) and ^{15}N dynamic nuclear polarization (DNP) solid-state NMR (SSNMR) experiments, in combination with plane-wave density functional theory (DFT) calculations of ^{14}N EFG tensors, were utilized to characterize a series of nitrogen-containing active pharmaceutical ingredients (APIs), including HCl salts of scopolamine, alprenolol, isoprenaline, acebutolol, dibucaine, nicardipine, and ranitidine. A case study applying these methods for the differentiation of polymorphs of bupivacaine HCl is also presented. All experiments were conducted upon samples with naturally-abundant nitrogen isotopes. For most of the APIs, it was possible to acquire frequency-stepped UW ^{14}N SSNMR spectra of stationary samples, which display powder patterns corresponding to pseudo-tetrahedral (*i.e.*, $\text{RR}'\text{R}''\text{NH}^+$ and $\text{RR}'\text{NH}_2^+$) or other (*i.e.*, RNH_2 and RNO_2) nitrogen environments. Directly-excited ^{14}N NMR spectra were acquired using the WURST-CPMG pulse sequence, which incorporates WURST (wideband, uniform rate, and smooth truncation) pulses and a CPMG (Carr-Purcell Meiboom-Gill) refocusing protocol. In certain cases, spectra were acquired using $^1\text{H} \rightarrow ^{14}\text{N}$ broadband cross-polarization, via the BRAIN-CP (broadband adiabatic inversion - cross polarization) pulse sequence. These spectra provide ^{14}N electric field gradient (EFG) tensor parameters and orientations that are particularly sensitive to variations in local structure and intermolecular hydrogen-bonding interactions. The $^1\text{H}\{^{15}\text{N}\}$ idHETCOR spectra, acquired under conditions of fast magic-angle spinning (MAS), used CP transfers to provide ^1H - ^{15}N chemical shift correlations for all nitrogen environments, except for two sites in acebutolol and nicardipine. One of these two sites ($\text{RR}'\text{NH}_2^+$ in acebutolol) was successfully detected using the DNP-enhanced $^{15}\text{N}\{^1\text{H}\}$ CP/MAS measurement, and one (RNO_2 in nicardipine) remained elusive due to the absence of nearby protons. This

exploratory study suggests that this combination of techniques has great potential for the characterization of solid APIs and numerous other organic, biological and inorganic systems.

1. Introduction

Most active pharmaceutical ingredients (APIs) are manufactured, shipped, stored and ingested as solids (ca. 80%).¹ Characterization of APIs is essential, providing important information on their molecular-level structures and corresponding relationships to their biological activity,² solubility,^{3,4} stability^{5,6} and bioavailability.⁵⁻⁷ In addition, approximately 80% of all solid APIs exhibit polymorphism or pseudopolymorphism (i.e., formation of hydrates and solvates). The identification and differentiation of polymorphic forms is of the utmost importance to the pharmaceutical industry as each polymorph may possess a unique set of physiochemical properties, which also has implications in patenting rights.⁸⁻¹¹

APIs and their associated polymorphs are most commonly characterized using techniques such as single-crystal or powder X-ray diffraction (scXRD, pXRD), as well as ¹H and ¹³C solid-state NMR (SSNMR).¹²⁻¹⁴ Several multinuclear SSNMR studies of APIs featuring other nuclides such as ²H, ¹¹B, ¹⁵N, ¹⁷O, ¹⁹F, ²³Na, ²⁷Al, ³¹P, and ⁷⁷Se have also been reported in recent years.¹⁵⁻³⁸ Furthermore, it has been recently demonstrated that ³⁵Cl SSNMR can provide important structural information about the chlorine sites in different polymorphic forms in APIs, including the nature of the hydrogen bonding environments and impurity phases, in reduced experimental times compared to conventional pXRD and ¹³C SSNMR experiments.^{24,32,39-41} For further reading on the use of SSNMR to characterize pharmaceutical compounds, we refer readers to recent reviews by Vogt and Monti *et al.*⁴²⁻⁴⁴

Given the ubiquity of nitrogen in functional groups such as amines, amides and numerous heterocycles, and the importance of intermolecular hydrogen-bonding interactions of nitrogen in solid APIs, the naturally occurring NMR-active nitrogen nuclei, ^{14}N and ^{15}N , could provide exclusive insights into their structures. Both nuclides yield NMR responses that are exceptionally sensitive to their local environments, and yet are among the most challenging isotopes for spectroscopic investigation by NMR (*vide infra*). Numerous studies employing ^{14}N and ^{15}N SSNMR, as well as quantum chemical computations, have recently been attempted for a variety of different compounds, including organic and biological samples,^{45–54} amino acids,^{55–62} and pharmaceuticals.^{27,63–69} ^{14}N nuclear quadrupole resonance (NQR) spectroscopy has also recently been applied, with some success, to a variety of APIs for purposes of quantification and polymorph differentiation.^{70–75}

The vast majority of SSNMR studies involving nitrogen have focussed upon the spin-1/2 ^{15}N nuclide, predominantly due to its relatively narrow spectral lines. However, owing to the inherently low natural abundance and low gyromagnetic ratio (γ) of ^{15}N , samples are typically isotopically enriched, which can be both costly and difficult to achieve. By contrast, there are far fewer ^{14}N (spin = 1) SSNMR studies,⁷⁶ due to an even lower value of γ , and more importantly, its large nuclear quadrupole moment ($Q = 20.44$ mbarn). The quadrupolar nature of ^{14}N nuclei is particularly challenging for SSNMR experimentation, as the first-order quadrupolar interaction can cause extreme broadening of ^{14}N SSNMR powder patterns, yielding Pake-like patterns which can span several MHz. This broadening occurs in cases where an aspherical ground-state electronic environment causes a sizeable electric field gradient (EFG) at the ^{14}N nucleus; in fact, this is the case for most systems, with the exception of ^{14}N nuclei in environments of very high spherical/Platonic symmetry, e.g., NH_4^+ ions.^{48,77}

A variety of techniques have been explored for the acquisition of ^{14}N SSNMR spectra, including the direct observation of ^{14}N NMR signals from single crystals,⁷⁸ ^{14}N magic-angle spinning (MAS) NMR using specialized probes with precisely tuned rotor angles,^{56,79} overtone ^{14}N MAS NMR,^{80–83} ^{14}N NMR enhanced by dynamic nuclear polarization (DNP)⁸⁴ and various indirect detection techniques.^{85–89} However, many of these techniques have not been widely adopted thus far owing to technical difficulties, costly hardware and/or issues relating to the nature of the nitrogen sites in samples under investigation. O'Dell and Cavadini recently provided thorough reviews of ^{14}N SSNMR experiments involving direct and indirect detection, respectively.^{76,90}

Recently, O'Dell, Schurko and co-workers^{58–60} demonstrated that comprehensive SSNMR structural studies of nitrogen-containing systems can be carried out using direct excitation of ^{14}N nuclei by means of the frequency-stepped WURST-CPMG protocol, which proved essential for the rapid acquisition of ^{14}N ultra-wideline (UW) SSNMR spectra.^{58,91–94} This protocol is comprised of three major components: (i) utilizing WURST (wideband, uniform rate, and smooth truncation) pulses⁹⁵ for uniform, direct excitation of broad powder patterns,⁹⁶ (ii) using CPMG (Carr-Purcell Meiboom-Gill) echo trains for enhancing the signal-to-noise ratio (S/N),⁹⁷ and (iii) stepping the transmitter in even increments across the breadth of the powder pattern (the 'frequency-stepped' method) to acquire sub-spectra at each frequency and subsequently generate the variable offset cumulative spectrum (VOCS).^{98,99} Successful utilization of the frequency-stepped WURST-CPMG sequence has been demonstrated for various spin-1/2^{100,101} and quadrupolar nuclei (integer and half-integer spins).^{62,94,102–108}

We recently demonstrated that the excitation of UW SSNMR spectra can be achieved using cross-polarization (CP) instead of direct excitation. The BRAIN-CP (broadband adiabatic

inversion CP) pulse sequence is utilized to enable polarization transfer over a wide frequency range (an order of magnitude larger than conventional CP experiments).¹⁰⁹ A major advantage of this sequence is the ability to perform efficient CP at low radio frequency (rf) power levels, making the sequence particularly attractive for NMR experiments involving low- γ nuclei with broad powder patterns, like ^{14}N . Several test cases of $^{14}\text{N}\{^1\text{H}\}$ BRAIN-CP-WCPMG NMR experiments have been presented for APIs, amino acids, and transition metal compounds.^{62,66,102}

In recent years there have also been significant advancements in the techniques utilized for the acquisition of ^{15}N SSNMR spectra. The availability of very fast MAS and the resulting boost in ^1H resolution offered opportunities for the indirect detection of ^{15}N nuclei (as well as the spectra of other dilute or low- γ nuclides).^{54,110,111} The technique, known as indirectly-detected heteronuclear correlation (idHETCOR) spectroscopy, has been successfully utilized in synthetic polymers and biopolymers,¹¹¹ organic-inorganic hybrid materials,¹¹² isotopically enriched proteins,¹¹³ peptides,^{54,114} and functionalized mesoporous silicas.^{115,116} Ishii and Tycko initially proposed a pulse sequence in which polarization transfers between ^1H and ^{15}N are achieved via adiabatic CP¹¹⁷ using a tangentially shaped pulse in the ^{15}N channel.¹¹⁰ A variation of this sequence was also recently proposed by Mao and Pruski, in which heteronuclear correlations are mediated through-bond.¹¹⁸ The indirect detection approach offers a sensitivity advantage exceeding one order of magnitude in comparison to conventional ^1H - ^{15}N HETCOR experiments,⁵⁴ thereby enabling routine acquisition of such spectra on *naturally abundant* samples without the need for costly ^{15}N isotopic labelling.

Another technique that is available for NMR studies of insensitive nuclei is the aforementioned DNP,^{119,120} which due to recent developments of gyrotron technology,¹²¹ low-temperature MAS probes¹²² and suitable biradical polarizing agents,^{123,124} has offered

enhancements of nuclear polarization exceeding two orders of magnitude in biological systems and various classes of materials.^{125–128} Current state-of-the-art DNP experiments in solids utilize the so-called cross effect, which relies on polarization exchange between three coupled spins, comprising two unpaired electrons, typically located in a single biradical molecule, and a nucleus. Measurements involving the detection of low- γ nuclei, such as ^{15}N , often involve an indirect route via protons, where the electron to ^1H transfer via DNP is followed by ^1H to ^{15}N transfer via CP. Several DNP CP/MAS studies of ^{15}N nuclei located on the surface and in the bulk of materials were recently reported.^{129–131}

Herein, we present a combined ^{14}N and ^{15}N SSNMR study of a series of naturally-abundant nitrogen-containing APIs and their associated polymorphic forms. It is demonstrated that investigating APIs using nitrogen NMR allows for accurate fingerprinting, differentiation and discovery of polymorphs via measurement of their unique chemical shift and quadrupolar NMR parameters, and also assists in the identification of impurity phases. We apply the WURST-CPMG and BRAIN-CP/WCPMG pulse sequences for the fast acquisition of UW ^{14}N SSNMR spectra at moderate (9.4 T) and high magnetic field strengths (21.1 T). We also show that the $^1\text{H}\{^{15}\text{N}\}$ idHETCOR technique is ideal for the measurement of the chemical shifts and through-space connectivities between ^1H and ^{15}N in APIs. Finally, we employ DNP-enhanced $^{15}\text{N}\{^1\text{H}\}$ CP/MAS measurements to detect the most elusive ^{15}N sites. Experimentally obtained ^{14}N EFG tensor parameters and ^{15}N chemical shifts are also compared to those derived from DFT calculations, and correlations between these parameters, tensor orientations and molecular-level structures are discussed. Commentary is provided on the potential application of these ^{14}N and ^{15}N SSNMR techniques for screening of bulk APIs and their dosage forms.

2. Experimental and Computational Details

2.1 Sample Preparation. All samples were purchased from Sigma-Aldrich and used without further purification. Schematic representations of the molecules, along with their abbreviations, are given in [Scheme 1](#). The polymorphic form of bupivacaine HCl, termed bupivacaine II HCl (**Bupi II**), was synthesized by heating bupivacaine HCl (**Bupi**) at 170 °C for 3 hours.^{39,132} To increase the ¹⁴N transverse relaxation time constants (T_2) for the **Bupi** samples (**I** and **II**), **Bupi** was partially deuterated by heating a saturated solution in 99.9% D₂O (Aldrich) at 80 °C for 1 hour. The D₂O was removed by slow evaporation and the samples were dried in a dessicator. Partially deuterated **Bupi II** was then synthesized following the same procedure as mentioned above.

2.2 X-ray Diffraction. To confirm the phase purity of each sample, powder X-ray diffraction (pXRD) experiments were carried out on a Bruker AXS HI-STAR system using a General Area Detector Diffractions system and CuK α ($\lambda = 1.540598 \text{ \AA}$) radiation. The experimentally obtained pXRD patterns were compared with theoretical pXRD patterns simulated using the PowderCell software package¹³³ based on previously reported crystal structure data.^{39,132,134–140} Full details on the pXRD patterns are provided in the Supporting Information.

2.3 ¹⁴N SSNMR. Moderate-field static ¹⁴N SSNMR experiments (i.e., performed on stationary samples) were conducted at 9.4 T on a wide-bore Oxford magnet equipped with a Varian Infinity Plus console, using a Larmor frequency of 28.88 MHz for ¹⁴N. Experiments were completed with a Varian/Chemagnetics double-resonance static HX probe fitted with a 5-mm coil and a low- γ tuning accessory. High-field static ¹⁴N NMR experiments were completed at the National Ultrahigh-Field NMR facility for Solids in Ottawa, on a Bruker 900 Avance II

spectrometer equipped with a standard-bore 21.1 T magnet, operated at a Larmor frequency of 65.03 MHz for ^{14}N . Experiments were completed using a home-built 7-mm static HX probe. The powdered samples were packed into shortened 5-mm and 7-mm glass NMR tubes. A sample of NH_4Cl (s) was used to calibrate the rf power on the ^{14}N channel. Due to the enormous breadths of the ^{14}N powder patterns, chemical shifts are not reported, as they have very large uncertainties.

As expected, the ^{14}N NMR powder patterns were too broad to be uniformly excited with a single high-power rectangular pulse of constant amplitude and phase; hence, they were acquired and processed using several UW techniques. For experiments involving direct excitation of the ^{14}N nuclei, the WURST-CPMG pulse sequence^{91,92} was applied, using an eight-step phase cycle and WURST-80 pulses⁹⁵ of equal amplitude and length for excitation and refocusing. $^1\text{H} \rightarrow ^{14}\text{N}$ CP NMR experiments were conducted using the BRAIN-CP-WCPMG pulse sequence.¹⁰⁹ In all cases, high-power proton decoupling was applied, with the decoupling RF fields between 30 and 82 kHz. Due to the limited excitation bandwidths associated with the WURST pulses, all spectra were acquired using the previously mentioned VOCS method,^{98,99} with frequency increments equal to an integer multiple of the spikelet spacings arising from the CPMG portion of the pulse sequence.¹⁴¹ The experimental times ranged from as long as 40 hours to as short as 8.4 hours, with a mean of approximately 16 hours. Further experimental details are given in the Supporting Information ([Tables S1 – S3](#)).

Processing of all ^{14}N SSNMR spectra was performed using the NUTS program from Acorn Software. Individual FIDs were Fourier transformed to produce sub-spectra, which were skyline-projected or co-added to produce the final spectrum. For all cases, except **Bupi** and **Bupi II**, only one half of the overall Pake-like pattern was acquired in both the direct excitation

and CP experiments. Under the assumption of a dominant first-order quadrupolar interaction, the total Pake-like pattern is centrosymmetric, and can be produced by ‘reflection’ or ‘mirroring’ of the high-frequency portion of the pattern about the center of the spectrum.⁵⁹ The positions of the three discontinuities in each half of the Pake-like pattern (i.e., the ‘foot’, ‘shoulder,’ and ‘horn’) depend directly on the values of C_Q and η_Q . These values do not depend on the exact positions or intensities of the individual spikelets, though the precision of their measurement is limited by the spikelet spacing. Alternatively, the echo train can be co-added and Fourier transformed to produce a continuous lineshape, as shown in [Figure S4](#). Analytical simulations of ^{14}N powder patterns were performed using the WSolids software package.¹⁴²

2.4 ^{15}N SSNMR. The 2D $^1\text{H}\{^{15}\text{N}\}$ idHETCOR experiments were performed at 14.1 T on a Varian NMR System spectrometer, equipped with a 1.6-mm triple-resonance FastMASTM probe and operated at 599.6 MHz for ^1H and 60.8 MHz for ^{15}N . All experiments were carried out under fast MAS at a rate of $\nu_{\text{rot}} = 40$ kHz using the idHETCOR pulse sequence shown in [Figure S5](#) and described in detail in earlier studies.⁵⁴ In short, the experiment commenced with $^1\text{H} \rightarrow ^{15}\text{N}$ CP transfer, followed by a t_1 period during which ^{15}N magnetization evolved in the presence of heteronuclear ^1H decoupling (SPINAL-64¹⁴³). Any residual ^1H magnetization remaining after the evolution period was eliminated using rotor resonance recoupling by a pair of long pulses with orthogonal phases,^{111,144} whose RF amplitudes satisfied the HORROR condition $\nu_{\text{RF}}(^1\text{H}) = \nu_{\text{rot}}/2$. The ^1H magnetization was detected following the final $^{15}\text{N} \rightarrow ^1\text{H}$ CP transfer, this time under heteronuclear ^{15}N SPINAL-64 decoupling. All spectra were acquired at ambient temperature and were processed using the GSim software package.¹⁴⁵ The ^{15}N nitrogen chemical shifts were referenced to nitromethane at -380.55 ppm (liquid ammonia at 0 ppm).¹⁴⁶

The DNP-enhanced $^{15}\text{N}\{^1\text{H}\}$ CP/MAS spectra of **Aceb** and **Nica** were obtained on a Bruker BioSpin DNP NMR spectrometer equipped with a 3.2-mm low-temperature MAS probe and a 263 GHz gyrotron, and operated at 400.3 MHz for ^1H and 40.6 MHz for ^{15}N . The samples were impregnated with a 16 mM 1,1,2,2-tetrachloroethane solution of TEKPol,¹²⁴ packed in a sapphire MAS rotor and spun at a MAS rate of 10 kHz and temperature of ~ 100 K. **Aceb** and **Nica** are insoluble in TCE, so there is no possibility of producing a new phase. For comprehensive lists of acquisition parameters used in $^1\text{H}\{^{15}\text{N}\}$ idHETCOR and DNP-enhanced $^{15}\text{N}\{^1\text{H}\}$ CP/MAS experiments we refer the reader to the Supporting Information ([Tables S4](#) and [S5](#), respectively).

2.5. Nomenclature. There are numerous pulse sequences applied in this work; for clarity, the following abbreviations are used herein: (1) ^{14}N UW spectra acquired with WURST-CPMG are denoted as ‘direct-excitation’ or ‘DE’; (2) the ^{14}N UW spectra obtained *via* BRAIN-CP/WURST-CPMG are denoted as ‘ $^{14}\text{N}\{^1\text{H}\}$ BCP’ or simply ‘BCP’; (3) the indirectly detected heteronuclear correlation spectra are denoted as ‘ $^1\text{H}\{^{15}\text{N}\}$ idHETCOR’ or ‘idHETCOR’; and (4) the spectra enhanced by dynamic nuclear polarization are referred to as ‘DNP $^{15}\text{N}\{^1\text{H}\}$ CP/MAS’ or ‘DNP CP/MAS’.

2.6. First-Principles Calculations. Calculations of NMR interaction tensors were completed using the CASTEP¹⁴⁷ DFT code in the Materials Studio 5.0 software suite. CASTEP is a plane-wave pseudopotential method that utilizes the gauge-including projector augmented wave (GIPAW) formalism.¹⁴⁸ The generalised gradient approximation (GGA) and revised Perdew, Burke and Ernzerhof (rPBE) functionals were used, with the core-valence interactions being described by on-the-fly pseudopotentials. Integrals over the Brillouin zone were performed using a Monkhorst-Pack grid with a k-point spacing of 0.08 \AA^{-1} . Wavefunctions were

expanded in plane waves, with kinetic energy less than a cut-off energy, typically 500 or 610 eV. Calculations output both the absolute shielding tensor, σ and the electric field gradient (EFG) tensor, \mathbf{V} , in the crystal frame. Crystal structures were obtained from the Cambridge Structural Database (CSD) and geometry optimization of the structure was performed (also within CASTEP in the Materials Studio software) prior to calculation of the NMR parameters. During geometry optimization of each structure only the proton positions were allowed to vary. Calculations were performed using the Shared Hierarchical Academic Research Computing Network (SHARCNET). Typical times for calculations ranged from 1 to 92 hours for geometry optimization and 8 to 110 hours for NMR calculations using 8, 16, 32, or 64 cores and 1, 2, or 4 GB of memory per core.

3. Results and Discussion

Below, the ^{14}N and ^{15}N SSNMR data are presented for each API, and discussed in terms of spectral features and the quadrupolar or chemical shift parameters extracted from each spectrum (these are given in Table 1). Following this, the experimentally measured and theoretically calculated ^{14}N quadrupolar parameters are correlated to the local structural environments of the nitrogen-containing moieties.

3.1 Nitrogen NMR of APIs. Before the NMR data for each API are discussed, we identify several common features for all ^{14}N SSNMR spectra. Using DE and BCP, it was possible to acquire ^{14}N SSNMR spectra of some of the nitrogen sites (see [Figures 1-3](#) and [5-7](#)) in reasonable time frames with high S/N and high resolution at 9.4 T and 21.1 T. Broad ^{14}N SSNMR powder patterns are observed at both fields, dominated by the quadrupolar interaction to first order, with negligible effects from the second-order quadrupolar interaction and chemical

shift anisotropy (Figure S6). It has been demonstrated by O'Dell *et al.* that nitrogen sites with pseudo-tetrahedral geometries possess much smaller values of C_Q (0.8 – 1.5 MHz) in comparison to those with pyramidal or planar geometries (2.8 – 4.0 MHz).⁵⁸⁻⁶⁰ We note that only the magnitude of C_Q , but not its sign, can be determined directly from the ^{14}N NMR spectra. Further discussion of the sign of C_Q (as determined by quantum chemical calculations) and its relation to molecular geometry is presented in section 3.2.2.

Given the extreme breadth of powder patterns associated with pyramidal or planar nitrogen sites, it is generally only feasible to probe pseudo-tetrahedral sites via DE ^{14}N SSNMR for the systems discussed herein, even though in some cases the signal arising from certain planar sites can be discerned in the baseline. We also note that considerable variation in CP efficiency is observed across the range of samples discussed below. Research is underway in our laboratory to access these much broader patterns via modified ^{14}N UW SSNMR experiments, including the effects of motion, relaxation mechanisms, and the various contributions to CP; further discussion of these topics is beyond the scope of the current work.

3.1.1 Scopolamine HCl. Scopolamine HCl (**Scop**) is used in the treatment of postoperative nausea and vomiting. Its crystal structure has a single nitrogen site with pseudo-tetrahedral geometry created by three nitrogen-carbon single bonds and one nitrogen-hydrogen single bond (Scheme 1a).¹³⁴ The ^{14}N DE spectrum (Figure 1a) was simulated with a single nitrogen environment, characterized by $C_Q = 1.29$ MHz and $\eta_Q = 0.29$ (see Table 1 for associated uncertainty values). These quadrupolar parameters are accurately determined from the positions of the previously mentioned discontinuities of the Pake-like pattern (the shoulder and horn); despite the fact that the third discontinuity at the edge (the foot) is not clearly resolved (see Figures S7 and S8 for additional information). In many cases, S/N in the outer foot region is

low, because there are fewer crystallites giving rise to observable signal. There is also the possibility that lower signal results from T_2 -dependent signal enhancement by CPMG refocusing, which differentiates spectral regions with distinct *effective* T_2 's, $T_2^{\text{eff}}(^{14}\text{N})$ (N.B.: the $T_2^{\text{eff}}(^{14}\text{N})$ is distinct from $T_2(^{14}\text{N})$ in that the contributions from heteronuclear dipolar coupling are wholly or partially removed by high-power ^1H decoupling for the former). In some cases, it was possible to enhance these spectral regions utilizing broadband CP methods;^{58–60,109} however, the $^{14}\text{N}\{^1\text{H}\}$ BCP experiment on **Scop** yielded very low S/N across the entire pattern; possible reasons for this include a short $T_{1\rho}$ for ^{14}N and/or ^1H , or slow build up of spin polarization for ^{14}N .

The $^1\text{H}\{^{15}\text{N}\}$ idHETCOR spectrum of **Scop** is shown in [Figure 1b](#) and displays a nitrogen resonance at $\delta_{\text{iso}} = -332$ ppm ([Table 1](#)) corresponding to a single nitrogen site, which is again in agreement with the crystal structure. This spectrum also reveals that the proton directly bound to nitrogen resonates at 8.4(5) ppm (throughout this work the uncertainties in the last decimal place of the proton chemical shifts are given in parentheses). Such correlations are extremely useful for structural characterization as they provide vital structural information regarding protons that are either directly bound or proximate in space to nitrogen.

3.1.2 Alprenolol HCl and Isoprenaline HCl. Alprenolol HCl (**Alpr**) is a non-cardioselective beta blocker, reported to have intrinsic sympathomimetic activity and some membrane-stabilizing properties. Isoprenaline HCl (**Isop**) is used in the treatment of slow heart rates and is structurally similar to adrenaline. **Alpr** and **Isop** each possess a single pseudo-tetrahedral $\text{RR}'\text{NH}_2^+$ nitrogen environment ([Scheme 1b](#) and [1c](#)).^{135,136} The $^{14}\text{N}\{^1\text{H}\}$ BCP spectrum of **Alpr** shown in [Figure 2a](#) has a much higher S/N than the DE spectrum (not shown), and was simulated with a single nitrogen environment: $C_Q = 1.13$ MHz and $\eta_Q = 0.82$. Again, the well-defined positions of the central horns and the overall pattern breadth allow for the

accurate measurement of the quadrupolar parameters, despite the fact that other singularities are difficult to distinguish (see [Figure S9](#)). Despite the structural similarity of **Isop** to **Alpr**, the acquisition of its ^{14}N NMR spectrum was considerably more challenging. It was not possible to observe any signal using DE methods; however, a $^{14}\text{N}\{^1\text{H}\}$ BCP spectrum was acquired ([Figure 2b](#)). The S/N in this spectrum is very poor, largely due to the short $T_2^{\text{eff}}(^{14}\text{N})$. We also note that a fair amount of background noise and interference is observed. Nonetheless, because of the clearly visible discontinuities, it was possible to simulate the spectrum, yielding quadrupolar parameters of $C_Q = 1.01$ MHz and $\eta_Q = 0.91$. Variable-temperature DE and BCP experiments were also attempted in an effort to increase $T_2^{\text{eff}}(^{14}\text{N})$ and thereby lengthen the CPMG echo trains;⁶² however, they were unsuccessful.

The $^1\text{H}\{^{15}\text{N}\}$ idHETCOR spectra for **Alpr** and **Isop**, shown in [Figures 2c](#) and [2d](#), respectively, both display single resonances in agreement with the reported crystal structures.^{134,136} The spectrum of **Alpr** features a single peak at $\delta_{\text{iso}} = -346$ ppm, which is strongly correlated with its directly bound protons ($\sim 4.9(5)$ ppm) and weakly correlated with the nearby CH_3 groups ($1.0(5)$ ppm). The idHETCOR spectrum of **Isop** displays a nitrogen resonance at $\delta_{\text{iso}} = -345$ ppm, which is also correlated with directly bound hydrogens ($6.3(5)$ ppm) and the nearby CH_3 groups ($0.5(5)$ ppm). The broad peak centered around 3-4 ppm, observed for both **Alpr** and **Isop**, corresponds to the nearby CH_2 groups.

Despite the structural similarities between **Alpr** and **Isop**, it is interesting to note that they show markedly different NMR responses in two respects: First, the pronounced differences in $T_2^{\text{eff}}(^{14}\text{N})$ make the acquisition of ^{14}N NMR spectra trivial for the former, and challenging for the latter. Second, notwithstanding their similar nitrogen chemical shifts, the dipolar correlations

observed in the $^1\text{H}\{^{15}\text{N}\}$ idHETCOR spectra are distinct from one another, revealing different spatial proximities between nitrogen and hydrogen.

3.1.3 Acebutolol HCl. Acebutolol HCl (**Aceb**) is a beta blocker typically used to treat high blood pressure and irregular heartbeats. It has two distinct nitrogen environments, one having pseudo-tetrahedral geometry ($\text{RR}'\text{NH}_2^+$) with two nitrogen-carbon single bonds and the other having planar geometry (Scheme 1d).¹³⁷ The UW ^{14}N powder pattern of **Aceb** is shown in Figure 3a and is indicative of the single pseudo-tetrahedral nitrogen environment. Simulation of the ^{14}N powder pattern yields $C_Q = 1.04$ MHz and $\eta_Q = 0.90$. In this instance, all three discontinuities are clearly resolved. As stated earlier, it is not possible to observe the full ^{14}N powder pattern corresponding to the planar nitrogen using the experimental conditions described in the Supporting Information. However, some signal intensity corresponding to these sites is visible on the outer edge of the powder pattern (marked with asterisks).

The $^1\text{H}\{^{15}\text{N}\}$ idHETCOR spectrum of **Aceb** (Figure 3b) displays a single cross-peak, in this case corresponding to nitrogen resonance at $\delta_{\text{iso}} = -250$ ppm and proton resonance at 8.7(5) ppm, which is assigned to the $\text{RR}'\text{NH}$ planar site. Efforts to observe the $\text{RR}'\text{NH}_2^+$ environment by increasing the spectral window and varying the contact time during CP were unsuccessful, which is surprising given that resonances of similar $\text{RR}'\text{NH}_2^+$ environments in both **Alpr** and **Isop** were clearly observed under similar conditions (*vide supra*). To verify the presence of both ^{15}N resonances, we resorted to DNP $^{15}\text{N}\{^1\text{H}\}$ CP/MAS measurement, which yielded two resonances at -250 ppm and -329 ppm (Figure 3c). DNP and idHETCOR experiments were conducted at 100 K and 298 K, respectively; since there is a good match between nitrogen chemical shifts that are observed in each spectrum, we are confident that the API has not undergone a phase transformation to a distinct polymorphic form.

3.1.4 Dibucaine HCl. Dibucaine HCl (**Dibu**) is a topical local anesthetic used to relieve pain and itching from burns, bites and stings. It has three distinct nitrogen sites in the unit cell; one having pseudo-tetrahedral geometry with three nitrogen-carbon single bonds ($\text{RR}'\text{R}''\text{NH}^+$), the second with planar geometry ($\text{RR}'\text{NH}$) and the third in an aromatic moiety (Scheme 1e).¹³⁸ Unfortunately, it was not possible to detect any of these sites using room- and variable-temperature DE and BCP ^{14}N NMR experiments. We hypothesize that strong heteronuclear ^1H - ^{14}N dipolar interactions are reducing the $T_2^{\text{eff}}(^{14}\text{N})$, thereby preventing the acquisition of a sufficient CPMG echo train; however, our attempts to reduce the dipolar interactions by high-power ^1H decoupling or partial deuteration were unsuccessful. A superficial comparison of the crystal structures of **Dibu** and other compounds for which ^{14}N SSNMR spectra are easily acquired does not reveal any obvious structural differences which can be correlated to this phenomenon.

All three nitrogen environments in **Dibu** are observed by the $^1\text{H}\{^{15}\text{N}\}$ idHETCOR method, with additional correlation information to multiple proton sites. Two distinct nitrogen resonances are observed in the $^1\text{H}\{^{15}\text{N}\}$ idHETCOR spectrum of **Dibu** (Figure 4) at $\delta_{\text{iso}} = -264$ ppm and $\delta_{\text{iso}} = -326$ ppm, which are correlated to their directly bound protons at 8.0(5) ppm and 10.7(5) ppm, and assigned to the planar and pseudo-tetrahedral nitrogen environments, respectively. The planar site is also weakly correlated to the proton in the neighbouring aromatic ring (8.6(5) ppm). Using the CP contact time of 3 ms (Table S4), it was not possible to observe the nitrogen in the aromatic group, as it does not have a directly bound proton. However, by increasing the CP contact time to 10 ms, we were able to observe this resonance at $\delta_{\text{iso}} = -135$ ppm (Figure S10), albeit at the expense of the S/N of the two other sites, which may be reduced due to fast $T_{1\rho}$ (^1H or ^{14}N) relaxation.

3.1.5 Nicardipine HCl. Nicardipine HCl (**Nica**) belongs to a class of calcium channel blockers and is used to treat high blood pressure and angina. There are three distinct nitrogen environments in **Nica**: one with pseudo-tetrahedral geometry ($RR'R''NH^+$), one with planar geometry ($RR'NH$), and one in a nitro group (RNO_2) of planar geometry ([Scheme 1f](#)).¹³⁹ The ^{14}N BCP powder pattern of **Nica** is shown in [Figure 5a](#) and is indicative of a single nitrogen environment, corresponding to the $RR'R''NH^+$ nitrogen site. Simulation of the ^{14}N powder pattern yielded $C_Q = 1.43$ MHz and $\eta_Q = 0.14$. Signal arising from the RNO_2 group is not observed in the ^{14}N BCP spectrum (even though the calculated C_Q is -1.10 MHz); this is likely due to the absence of directly bound or proximate protons (the nearest proton is *ca.* 2.66 Å away from the nitrogen).

The idHETCOR spectrum in [Figure 5b](#) displays two distinct ^{15}N resonances at -265 ppm and -348 ppm, which are assigned to the planar ($RR'NH$) and pseudo-tetrahedral nitrogen environments, respectively. The resonance at $\delta_{iso} = -265$ ppm displays a strong correlation at 9.2(5) ppm corresponding to the proton directly bound to the planar nitrogen ($RR'NH$), and a much weaker correlation at 3.4(5) ppm attributed to protons in the CH_3 group adjacent to the NH group ([Scheme 1f](#)). The pseudo-tetrahedral nitrogen resonating at $\delta_{iso} = -348$ ppm exhibits detectable interactions with several proton sites. The correlation at 3.4(5) ppm belongs to the protons in the adjacent CH_3 group, the broad low-intensity peak in the range between 5 and 7 ppm corresponds to the nearby CH_2 groups, and the peak at 7.9(5) ppm is due to the aromatic hydrogen atoms. The weaker correlation observed at 11.4(5) ppm is assigned to the hydrogen atoms directly bonded to the pseudo-tetrahedral nitrogen. Its low intensity is most likely due to fast $T_{1\rho}$ relaxation processes, which may have attenuated this resonance during two CP transfers, each lasting 3 ms.

It is noted that the RNO₂ group in **Nica** is not observed in the idHETCOR spectrum, even at a longer CP contact time of 10 ms. As in the case of **Aceb**, we carried out a DNP CP/MAS measurement of this sample (Figure 5c), which also failed to produce any new resonances in addition to those at -265 ppm and -348 ppm. The ¹H → ¹⁵N CP process is clearly not efficient enough to yield any discernible signal from the RNO₂ moiety, at both 100 and 298 K. As in the case of **Aceb**, matching nitrogen chemical shifts in the DNP and idHETCOR spectra indicate that no polymorphic transformation has taken place.

3.1.6 Ranitidine HCl. Ranitidine HCl (**Rani**) is a histamine H₂-receptor antagonist that inhibits stomach acid production and is commonly used in the treatment of peptic ulcer disease. **Rani** has four distinct nitrogen environments in the unit cell: one with pseudo-tetrahedral geometry (RR'R''NH⁺), two with planar geometries (RR'NH) and one in a nitro group (RNO₂) (Scheme 1g).¹⁴⁰ The ¹⁴N BCP spectrum of **Rani** is shown in Figure 6a. Remarkably, powder patterns corresponding to all four sites are present, and simulated with values of C_Q = 1.15, 1.62, 3.25 and 3.25 MHz and η_Q = 0.49, 0.22, 0.50 and 0.58, respectively (see Figures S11 and S12 for detailed information regarding this simulation). ¹⁴N EFG tensors obtained from DFT calculations greatly aided in the fitting process.

The ¹H{¹⁵N} idHETCOR spectrum of **Rani** (Figure 6b) also has four distinct resonances, associated with RR'R''NH⁺ (δ_{iso} = -340 ppm), RR'NH (δ_{iso} = -292 and -281 ppm), and RNO₂ (δ_{iso} = -22 ppm) nitrogen environments.¹⁴⁰ These assignments are corroborated by the observed correlations with the directly bound hydrogen atoms at 11.4(5) ppm (RR'R''NH⁺) and 9.4(5) ppm (both RR'NH sites). The resonance at δ_{iso} = -281 ppm is assigned to the planar RR'NH nitrogen environment near the end of the alkyl chain (labelled site 1 in Figure S13). The resonance at δ_{iso} = -292 ppm belongs to the second planar nitrogen (labelled site 2 in Figure S13) because it also

exhibits a weak correlation with the adjacent CH₂ group (7.4(5) ppm). The resonance at $\delta_{\text{iso}} = -22$ ppm corresponds to the nitro group that does not possess any directly bound protons, and is correlated to a proton in the adjacent ethylene group.

The characterization of **Rani** benefits significantly from the tandem ¹⁴N and ¹⁵N NMR techniques. Typically, only the pseudo-tetrahedral nitrogen sites are observed in ¹⁴N SSNMR spectra at moderate magnetic fields (i.e., 9.4 T); however, in this case, the BCP experiment makes it possible to see contributions from all of the crystallographically distinct ¹⁴N nuclei. In addition, in the ¹H{¹⁵N} idHETCOR spectra, all four of the nitrogen environments are observed, providing important heteronuclear correlation information that aids in structural assignment.

3.1.7. Bupivacaine HCl and its Polymorphs. Bupivacaine HCl is a local anesthetic and is one of many APIs that exhibit polymorphism. There are several known polymorphs of bupivacaine HCl; in this study we are focusing upon the main form, bupivacaine HCl (**Bupi**), which is the bulk form obtained from Sigma-Aldrich (and also found in dosage forms),³⁹ and the polymorph known as bupivacaine II HCl (**Bupi II**).¹³² **Bupi** and **Bupi II** each have two nitrogen environments: one with planar geometry, and the other with pseudo-tetrahedral geometry formed by one N-H bond and three nitrogen-carbon single bonds ([Scheme 1h](#)).^{39,132} The planar sites are expected to have large values of C_Q , as confirmed by DFT calculations (*vide infra*), and are not observed.

¹⁴N UW NMR spectra of **Bupi** and **Bupi II** were acquired at 9.4 T ([Figures S14 and S15](#), respectively) and 21.1 T ([Figure 7](#)). The spectral discontinuities at the horn, shoulder, and foot positions are very well defined at 21.1 T, enabling differentiation between the two polymorphs. Each of the ¹⁴N powder patterns was simulated with a single nitrogen site corresponding to the pseudo-tetrahedral environment, yielding $C_Q = 1.00$ MHz, $\eta_Q = 0.30$ and $C_Q = 1.25$ MHz, $\eta_Q =$

0.19, for **Bupi** and **Bupi II**, respectively. It is noted that there is underlying signal intensity corresponding to the second nitrogen site in both ^{14}N SSNMR spectra as well as in the 9.4 T spectra of **Bupi** (Figure S14). In these cases, the favourable relaxation characteristics (i.e., short $T_1(^{14}\text{N})$ and long $T_2^{\text{eff}}(^{14}\text{N})$) of the planar nitrogen site seem to allow for its detection, even at moderate magnetic fields; however, we did not obtain the entire ^{14}N UW spectrum for this site – this will be the subject of future investigations.

Each of the $^1\text{H}\{^{15}\text{N}\}$ idHETCOR spectra of **Bupi** and **Bupi II** (Figures 8a and 8b) feature two distinct nitrogen resonances: $\delta_{\text{iso}} = -342$ ppm and $\delta_{\text{iso}} = -269$ ppm for **Bupi** and $\delta_{\text{iso}} = -345$ ppm and $\delta_{\text{iso}} = -267$ ppm for **Bupi II**, which are assigned to the pseudo-tetrahedral and planar sites, in each case. All of these resonances show strong correlations with their directly bound hydrogen atoms: at 10.0(5) and 10.7(5) ppm for the pseudo-tetrahedral sites, and at 10.8(5) ppm and 12.1(5) ppm for the planar sites in **Bupi** and **Bupi II**, respectively. Several weaker correlations are also observed in both polymorphs, between the nitrogen sites and their adjacent aliphatic protons.

3.1.8. Summary of ^{14}N and ^{15}N SSNMR data. For most samples, ^{14}N SSNMR spectra are dominated by powder patterns corresponding to pseudo-tetrahedral nitrogen environments, due to their reduced values of C_Q and correspondingly narrower powder patterns. There are some exceptions, where either the relaxation and/or the CP conditions enable the rapid acquisition of broader patterns (e.g., **Rani**) or prevent acquisition altogether (e.g., **Dibu**). Nonetheless, the exclusive observation of the nitrogen patterns corresponding to pseudo-tetrahedral sites is extremely useful for the differentiation of polymorphs (see Section 3.1.7), because the ^{14}N EFG tensors are very sensitive to different hydrogen bonding configurations (much more so than nitrogen chemical shifts in many instances). The ^{14}N SSNMR spectra yield

η_Q values that are closer to zero or one for $RR'R''NH^+$ or $RR'NH_2^+$ environments, respectively. A particularly valuable aspect of having experimentally determined ^{14}N EFG tensors is the ease with which they can be modeled via quantum chemical computations; the relationships between local symmetries and EFG tensor parameters and orientations are discussed in *Section 3.2*.

The majority of nitrogen sites in these APIs were observed using $^1H\{^{15}N\}$ idHETCOR spectroscopy. Two sites did not polarize well under CP (note that the idHETCOR pulse sequence uses two CP processes), $RR'NH_2^+$ in **Aceb** and RNO_2 in **Nica**; however, the former was identified using the DNP-enhanced $^{15}N\{^1H\}$ CP/MAS method. The $^1H\{^{15}N\}$ idHETCOR spectra provide more structural insights about the APIs than are typically obtained in conventional ^{15}N solution NMR spectra, i.e., it is not simply a matter of observing the different nitrogen environments, but rather, collecting much richer structural information on intermolecular interactions, hydrogen bonding, and conformational differences. These 2D spectra also have potential for polymorph fingerprinting and differentiation. Indeed, distinct 1H and ^{15}N chemical shifts are observed in **Bupi** and **Bupi II**, highlighting the subtle structural differences between the two polymorphs.

3.2. Plane-wave DFT Calculations of NMR Interaction Tensors. Plane-wave DFT calculations of ^{14}N EFG tensor parameters and nitrogen nuclear magnetic shielding (NMS) parameters were conducted on models derived from known crystal structures for each API.^{39,132,134–140} DFT calculations were completed using the CASTEP software package¹⁴⁷ (see Experimental Section for details). Molecular systems involved in strong intermolecular hydrogen-bonding interactions typically require structural optimization prior to calculation of the NMR parameters. In particular, it is almost always necessary to optimize the hydrogen atom positions in the absence of neutron diffraction data. In addition, it is noted that several of the

pharmaceuticals discussed herein have extremely large unit cells containing a large number of atoms, which can be problematic for plane-wave calculations.

3.2.1 Experiment vs. Theory. The calculated ^{14}N EFG tensor parameters and isotropic NMS values obtained after optimization of the hydrogen atom positions in each structure are listed in [Table 1](#). Given the limited number of systems, the variety of nitrogen environments, and the great variability in unit cell sizes, quality of crystal structures and temperatures of XRD experiments, overarching statements regarding the accuracy of the calculations cannot be made. There is reasonably close agreement between the experimental and theoretical values of C_Q and η_Q ; in particular, the asymmetry parameters are extremely useful for differentiating distinct bonding environments in the pseudo-tetrahedral nitrogens (*vide infra*). In order to draw correlations between experimental and theoretical chemical shifts, a more detailed study involving comparison of chemical shift and NMS tensors must be made. This is beyond the scope of the current study; nonetheless, the preliminary set of nitrogen NMS calculations are presented in this work. The remainder of this section focuses only upon the ^{14}N EFG tensors. A complete summary of all EFG and NMS tensor parameters is given in [Table S6](#).

3.2.2 ^{14}N EFG Tensor Orientations and the Sign of C_Q . By examining the ^{14}N EFG tensor orientations obtained from DFT calculations, it is possible to make correlations between the experimentally measured tensor parameters and known molecular structures and local symmetries. This aids in understanding the origins of the ^{14}N quadrupolar interactions and their relation to molecular structure, and provides an attractive means of making structural predictions for systems with hitherto unknown structures. The signs of the components of the EFG tensor also show variation with differences in bonding and structure, and are intimately related to the tensor orientations. Since $C_Q = eQV_{33}/h$, C_Q and V_{33} have the same signs for ^{14}N , since the value

of eQ is positive. Furthermore, since the EFG tensor is traceless (i.e., $V_{11} + V_{22} + V_{33} = 0$), the signs of V_{11} and V_{22} are always opposite to that of V_{33} . It is important to note that the sign of C_Q cannot be determined directly from a ^{14}N NMR spectrum, but can be determined from J - and dipolar spin pairs subject to a variety of single- and double-resonance experiments.^{90,149}

The ^{14}N EFG tensor in **Scop** has V_{33} oriented near the direction of the N-H bond ($\angle(V_{33}\text{-N-H}) = 10.19^\circ$), which is typical for $\text{RR}'\text{R}''\text{NH}^+$ pseudo-tetrahedral nitrogen environments (Figure 9a).⁵⁹ The orientations of V_{11} and V_{22} can vary for such environments, and the value of η_Q indicates that these components are similar in magnitude. For the $\text{RR}'\text{NH}_2^+$ nitrogen environments in **Alpr** and **Isop**, the high values of η_Q indicate that the magnitudes of V_{22} and V_{33} are similar (but opposite in sign), and that V_{11} is the distinct component of the EFG tensor. V_{33} is oriented in a direction approximately perpendicular to the H-N-H plane in each case ($\angle(V_{33}\text{-N-H}_A) = 93.00^\circ$ and $\angle(V_{33}\text{-N-H}_A) = 97.81^\circ$, respectively) and V_{11} is oriented between the two hydrogen atoms in the same plane, approximately bisecting the H-N-H angle (Figures 9b and 9c).⁵⁹ The calculated values of C_Q for these $\text{RR}'\text{R}''\text{NH}^+$ and $\text{RR}'\text{NH}_2^+$ environments are negative and positive, respectively, which means that negative EFGs are observed in the direction/plane of covalent N-H bonds, and positive EFGs are observed perpendicular to these bonds.

For the $\text{RR}'\text{NH}_2^+$ nitrogen environment in **Aceb**, V_{22} is oriented perpendicular to the H-N-H plane ($\angle(V_{33}\text{-N-H}_A) = 98.91^\circ$, Figures 10a and 10b), rather than V_{33} (as in the cases of **Alpr** and **Isop**). In addition, the sign of the C_Q is opposite to those of **Alpr** and **Isop**. However, the signs of the EFGs in **Aceb** are the same as those in **Alpr** and **Isop**: positive and negative in directions perpendicular and parallel to the H-N-H plane, respectively. Since V_{22} and V_{33} are similar in magnitude (but opposite in sign), the change in sign of C_Q is not as dramatic a difference in tensor orientation as one would think; rather, the absolute magnitudes of the

negative EFGs are greater than those of the positive EFGs in **Aceb**; the reverse is true for **Alpr** and **Isop**.

The three-coordinate, planar RR'NH nitrogen moiety in **Aceb** is structurally and electronically distinct from the aforementioned pseudo-tetrahedral sites (R and R' correspond to the aromatic and carbonyl moieties, [Figure 10c](#)). V_{33} is directed approximately perpendicular to the C_{Ar} -N- C_{CO} plane ($\angle(V_{33}\text{-N-}C_{Ar}) = 82.52^\circ$), while V_{11} is slightly below this plane and near the N-H bond ($\angle(V_{11}\text{-N-H}) = 13.96^\circ$). Here, V_{33} is the distinct tensor component, indicating a large negative EFG along the direction of the nitrogen p_z orbital, in agreement with previous observations.^{59,150,151}

There are three distinct nitrogen-containing moieties in **Nica**, and as such, three unique ^{14}N EFG tensors. Despite the fact that only the ^{14}N pattern for the pseudo-tetrahedral RR'R''NH⁺ moiety is observed, the tensor orientations are still of interest, and can be compared to those of **Rani** (*vide infra*). The RR'R''NH⁺ and planar RR'NH moieties have tensor orientations and EFG signs akin to those described above ([Figures 11a](#) and [11b](#)): the former has V_{33} (negative EFG) oriented near the N-H bond ($\angle(V_{33}\text{-N-H}) = 3.67^\circ$), and the latter has V_{33} (negative EFG) perpendicular to the C-N-C plane and V_{11} close to the N-H bond. The planar RNO₂ group has V_{11} oriented approximately perpendicular to the O-N-O plane, and V_{33} near the direction of the C-N bond ($\angle(V_{33}\text{-N-C}) = 1.14^\circ$, [Figure 11c](#)).

Rani has four distinct nitrogen-containing moieties that all give rise to unique ^{14}N EFG tensors. The ^{14}N EFG tensor of the RR'R''NH⁺ moiety has a similar orientation to that described above for **Nica** and **Scop**; V_{33} is oriented nearly along the N-H bond ($\angle(V_{33}\text{-N-H}) = 1.18^\circ$, [Figure 12a](#)). The RR'NH moieties have tensor orientations and EFG signs that are also consistent with those described above: V_{33} is oriented nearly perpendicular to the C-N-C plane and V_{11}

approximately bisects the C-N-C angle (Figure 12b). The RNO₂ moiety has an EFG tensor orientation with V_{11} oriented perpendicular to the O-N-O plane ($\angle(V_{11}\text{-N-O}) = 88.04^\circ$) and V_{22} oriented nearly coincident with the C-N bond ($\angle(V_{22}\text{-N-C}) = 7.57^\circ$) (unlike V_{33} in **Nica**).

To date, the ¹⁴N EFG tensors of RNO₂ groups have only been investigated by a handful of researchers, including by Cox *et al.* (nitromethane using microwave spectroscopy),^{152,153} Subbarao *et al.* (a series of aromatic nitro compounds with ¹⁴N NQR and Townes-Dailey theory)¹⁵⁴ and Harris *et al.* (nitrobenzene via ¹³C-¹⁴N residual dipolar couplings measured in ¹³C CP/MAS NMR spectra).¹⁵⁵ The current work on **Nica** and **Rani** represents a modern instance of the application electronic structure calculations on periodic solids to examine this class of ¹⁴N EFG tensors. Interestingly, previous work has shown great variation in the ¹⁴N EFG tensor orientations and the signs of C_Q , which may result from not only differences in local molecular structures, but also because of intermolecular hydrogen bonding in solids.¹⁵⁴ Clearly, more work is necessary to examine the variations of these tensors with structure, especially in condensed phases; for now, we have summarized the full set of results in a simple diagram (Figure S19).

Finally, the ¹⁴N EFG tensors for **Bupi** and **Bupi II** are shown in Figure 13. The tensor orientations for the pseudo-tetrahedral RR'R''NH⁺ moieties (Figure 13a and 13c) are consistent with those of other RR'R''NH⁺ groups, with V_{33} (negative EFG) being oriented nearly along the N-H bond ($\angle(V_{33}\text{-H-N}) = 8.35^\circ$ for **Bupi** and $\angle(V_{33}\text{-H-N}) = 17.40^\circ$ for **Bupi II**). For the planar RR'NH groups (Figures 13b and 13d), tensor orientations feature V_{33} (negative) oriented nearly perpendicular to the C-N-C plane ($\angle(V_{33}\text{-N-C}_{Ar}) = 86.25^\circ$ for **Bupi** and $\angle(V_{33}\text{-N-C}_{Ar}) = 111.58^\circ$ for **Bupi II**) and V_{11} is close to the direction of the N-H bond ($\angle(V_{11}\text{-H-N}) = 8.64^\circ$ for **Bupi** and $\angle(V_{11}\text{-H-N}) = 9.05^\circ$ for **Bupi II**).

3.2.3 Summary of ^{14}N EFG tensor orientations. For pseudo-tetrahedral $\text{RR}'\text{R}''\text{NH}^+$ nitrogen environments, V_{33} is found to be near the direction of the N-H bond, the η_Q is low (i.e., < 0.30), and the sign of C_Q is negative. For pseudo-tetrahedral $\text{RR}'\text{NH}_2^+$ nitrogen moieties, the η_Q is close to one, and the sign of C_Q is positive if V_{33} is oriented nearly perpendicular to the H-N-H plane (e.g., **Alpr** and **Isop**), and negative if V_{22} is oriented perpendicular to the H-N-H plane rather than V_{33} (e.g., **Aceb**), resulting in a negative value of C_Q . For planar $\text{RR}'\text{NH}$ nitrogen sites, C_Q is negative, with V_{11} oriented close to the N-H bond and V_{33} approximately perpendicular to the C-N-C plane. Finally, for planar RNO_2 nitrogen sites, V_{11} is oriented perpendicular to the O-N-O plane. There is some variation in the orientations of V_{22} and V_{33} , which may result from intermolecular interactions; however, the signs of the EFGs along and perpendicular to the C- NO_2 bond are always negative and positive, respectively.

4. Conclusions

We have demonstrated that the combined use of ^{14}N and ^{15}N SSNMR methods, including DE, BCP, $^1\text{H}\{^{15}\text{N}\}$ idHETCOR and DNP, in conjunction with plane-wave DFT calculations of ^{14}N EFG tensors, can provide sets of NMR parameters needed for comprehensive structural characterization of nitrogen-containing APIs. It was found that our UW ^{14}N methods favor the observation of signals arising from pseudo-tetrahedral nitrogen moieties, due to their smaller values of C_Q (ca. 1 – 1.5 MHz) and correspondingly narrower patterns in comparison to those of ^{14}N nuclei in planar nitrogen environments. These patterns enable accurate determinations of C_Q and η_Q , which are found to be extremely sensitive to even the most subtle structural differences, including distinct hydrogen bonding configurations. The $^1\text{H}\{^{15}\text{N}\}$ idHETCOR method proved instrumental in providing important chemical shift and spatial correlation information in natural

abundance samples. In most cases, well-resolved peaks and correlations corresponding to multiple nitrogen environments of different geometries were observed, even for sites with no directly bound hydrogen atoms. By using ^{14}N and ^{15}N SSNMR in tandem, it is possible to accurately distinguish between different polymorphic forms of APIs, as demonstrated for bupivacaine HCl. Plane-wave DFT calculations provide additional important information on the relationships between the ^{14}N EFG tensors, the signs of the EFGs, and the molecular structures of the APIs.

This work represents a first exploratory effort in using tandem ^{14}N and ^{15}N SSNMR methods for studying APIs. First, further work must be done on enhancing the performance of the ^{14}N and ^{15}N NMR experiments. For the former, the development of new protocols for broadband cross polarization, efficient ^1H decoupling, and uniform excitation with broadband pulses are all crucial. Investigation of the use of ^{14}N static NMR experiments under DNP conditions would also be of great interest, perhaps for accessing some of the extremely broad patterns arising from planar nitrogen sites (e.g., $\text{RR}'\text{NH}$). In addition, ^{14}N NMR experiments that are targeted at enhancing selection regions of the powder patterns (as opposed to the full patterns) may also have great utility in this regard. For the latter, the use of advanced ultra-fast MAS probes (i.e., rotation speeds of 100+ kHz)¹⁵⁶⁻¹⁵⁸ may further refine the idHETCOR experiments in terms of resolution in the ^1H dimension, and the use of enhanced ^1H decoupling schemes may allow for the use of larger rotor sizes for increased S/N. Projects focused on addressing these issues are currently underway in our laboratories. Second, efforts must be made to ameliorate agreement between experimental and theoretical NMR tensor parameters. Full geometry optimizations, better density functionals, the use of superior basis sets, and the inclusion of dispersion effects,¹⁵⁹ may all be of value. Given such improvements, it is possible

that $^{14/15}\text{N}$ NMR data sets obtained with our methods may be useful in the emerging area of NMR crystallography,¹⁶⁰ where structural predictions can be made with computational methods including *ab initio* random structural searching (AIRSS) algorithm¹⁶¹⁻¹⁶⁴ and other algorithms,¹⁶⁵⁻¹⁶⁷ and refined with the aid of high-quality NMR data.

Finally, we hope that this work encourages others to consider applying the methodologies for ^{14}N and ^{15}N SSNMR presented herein, for not only study of APIs (i.e., polymorph differentiation, impurity detection, and discovery of new structures in both bulk and dosage forms), but also to a wide assortment of organic, biological, inorganic, and organometallic nitrogen-containing systems.

Acknowledgements

R.W.S. acknowledges the Natural Science and Engineering Research Council (NSERC, Canada) for support in the form of Discovery, Accelerator, and Research Tools and Instruments (RTI) grants. He also acknowledges the University of Windsor for a 50th Golden Jubilee Research Award. S.L.V. thanks the province of Ontario for a Queen Elizabeth II – Graduate Scholarship in Science and Technology as well as an Ontario Graduate Scholarship. We are grateful to the Canadian Foundation for Innovation (CFI), the Ontario Innovation Trust (OIT), and the University of Windsor for supporting our NMR spectroscopy and X-ray facilities. Experiments at 21.1 T were conducted at the Canadian National Ultrahigh-Field NMR facility for Solids (www.nmr900.ca). Drs. Victor Terskikh, Eric Ye, Luke O’Dell, Kris Harris, and Bryan Lucier are thanked for their assistance with all experiments at 21.1 T. In addition, Mr. Jamie Bennett (NRC, Ottawa) is thanked for construction of the 7-mm double resonance probe used for all experiments at 21.1 T. Computational work described herein was made possible by the facilities of the Shared Hierarchical Academic Research Computing Network (SHARCNET: www.sharcnet.ca). At the Ames Laboratory, this research is supported by the U.S. Department of Energy (DOE), Office of Science, Basic Energy Sciences, Division of Chemical Sciences, Geosciences, and Biosciences. Ames Laboratory is operated for the DOE by Iowa State University under Contract No. DE-AC02-07CH11358.

References

- 1 M. Geppi, G. Mollica, S. Borsacchi and C. A. Veracini, *Appl. Spectrosc. Rev.*, 2008, **43**, 202–302.
- 2 D. Giron, *J. Therm. Anal. Calorim.*, 2003, **73**, 441–457.
- 3 S. R. Byrn, R. R. Pfeiffer, G. A. Stephenson, D. J. W. Grant and W. B. Gleason, *Chem. Mater.*, 1994, **6**, 1148–1158.
- 4 D. Giron, *J. Therm. Anal. Calorim.*, 2001, **64**, 37–60.
- 5 D. Giron, *Am. Pharm. Rev.*, 2005, **8**, 32.
- 6 D. Giron, *Am. Pharm. Rev.*, 2005, **8**, 72.
- 7 D. Giron, in *Lipophilicity Symposium*, Zurich, 2006, p. 307.
- 8 H. G. Brittain, *Polymorphism in Pharmaceutical Solids*, Marcel Dekker, New York, 1999, vol. 95.
- 9 J. K. Halebian and W. McCrone, *J. Pharm. Sci.*, 1969, **58**, 911–929.
- 10 P. H. Karpinski, *Chem. Eng. Technol.*, 2006, **29**, 233–238.
- 11 A. Llinàs, K. J. Box, J. C. Burley, R. C. Glen and J. M. Goodman, *J. Appl. Crystallogr.*, 2007, **40**, 379–381.
- 12 R. K. Harris, *Analyst*, 2006, **131**, 351–373.
- 13 R. K. Harris, *J. Pharm. Pharmacol.*, 2007, **59**, 225–239.
- 14 M. Geppi, G. Mollica, S. Borsacchi and C. A. Veracini, *Appl. Spectrosc. Rev.*, 2008, **43**, 202–302.
- 15 V. Chupin, A. I. P. M. de Kroon and B. de Kruijff, *J. Am. Chem. Soc.*, 2004, **126**, 13816–13821.
- 16 J. M. Griffin, D. R. Martin and S. P. Brown, *Angew. Chemie - Int. Ed.*, 2007, **46**, 8036–8038.
- 17 Z. J. Li, Y. Abramov, J. Bordner, J. Leonard, A. Medek and A. V Trask, *J. Am. Chem. Soc.*, 2006, **128**, 8199–210.
- 18 E. D. L. Smith, R. B. Hammond, M. J. Jones, K. J. Roberts, J. B. O. Mitchell, S. L. Price, R. K. Harris, D. C. Apperley, J. C. Cherryman and R. Docherty, *J. Phys. Chem. B*, 2001, **105**, 5818–5826.
- 19 F. G. Vogt, J. Brum, L. M. Katrincic, A. Flach, J. M. Socha, R. M. Goodman and R. C. Haltiwanger, *Cryst. Growth Des.*, 2006, **6**, 2333–2354.
- 20 I. Wawer, D. M. Pisklak and Z. Chilmonczyk, *J. Pharm. Biomed. Anal.*, 2005, **38**, 865–870.
- 21 R. M. Wenslow, *Drug Dev. Ind. Pharm.*, 2002, **28**, 555–561.
- 22 F. G. Vogt, H. Yin, R. G. Forcino and L. Wu, *Mol. Pharm.*, 2013, **10**, 3433–3446.
- 23 A. J. Rossini, C. M. Widdifield, A. Zagdoun, M. Lelli, M. Schwarzwälder, C. Copéret, A.

- Lesage and L. Emsley, *J. Am. Chem. Soc.*, 2014, **136**, 2324–2334.
- 24 F. G. Vogt, G. R. Williams, M. Strohmeier, M. N. Johnson and R. C. B. Copley, *J. Phys. Chem. B*, 2014, **118**, 10266–10284.
- 25 N. M. Dicaire, F. A. Perras and D. L. Bryce, *Can. J. Chem.*, 2014, **92**, 9–15.
- 26 X. Kong, M. Shan, V. V. Terskikh, I. Hung, Z. Gan and G. Wu, *J. Phys. Chem. B*, 2013, **117**, 9643–9654.
- 27 P. Przybylski, K. Pyta, K. Klich, W. Schilf and B. Kamieński, *Magn. Reson. Chem.*, 2014, **52**, 10–21.
- 28 K. Paradowska and I. Wawer, *J. Pharm. Biomed. Anal.*, 2014, **93**, 27–42.
- 29 F. G. Vogt, P. C. Dell’Orco, A. M. Diederich, Q. Su, J. L. Wood, G. E. Zuber, L. M. Katrincic, R. L. Mueller, D. J. Busby and C. W. DeBrosse, *J. Pharm. Biomed. Anal.*, 2006, **40**, 1080–1088.
- 30 H. G. Brittain, K. R. Morris, D. E. Bugay, A. B. Thakur and a. T. M. Serajuddin, *J. Pharm. Biomed. Anal.*, 1993, **11**, 1063–1069.
- 31 K. M. N. Burgess, F. A. Perras, A. Lebrun, E. Messner-Henning, I. Korobkov and D. L. Bryce, *J. Pharm. Sci.*, 2012, **101**, 2930–2940.
- 32 F. G. Vogt, G. R. Williams and R. C. B. Copley, *J. Pharm. Sci.*, 2013, **102**, 3705–3716.
- 33 S. L. Hem and C. T. Johnston, *Production and Characterization of Aluminum-Containing Adjuvants*, John Wiley & Sons, Inc., Hoboken, NJ, USA, 1st edn., 2015.
- 34 Y.-H. Kiang, K. Nagapudi, T. Wu, M. L. Peterson, J. Jona, R. J. Staples and P. W. Stephens, *J. Pharm. Sci.*, 2015, **104**, 2161–2168.
- 35 X. Kong, V. V. Terskikh, A. Toubaei and G. Wu, *Can. J. Chem.*, 2015, **93**, 1–9.
- 36 J. Liu, K. Nagapudi, Y.-H. Kiang, E. Martinez and J. Jona, *Drug Dev. Ind. Pharm.*, 2009, **35**, 969–75.
- 37 M. Skotnicki, D. C. Apperley, J. A. Aguilar, B. Milanowski, M. Pyda and P. Hodgkinson, *Mol. Pharm.*, 2016, **13**, 211–222.
- 38 F. G. Vogt, K. Roberts-Skilton and S. A. Kennedy-Gabb, *Pharm. Res.*, 2013, **30**, 2315–2331.
- 39 H. Hamaed, J. M. Pawlowski, B. F. T. Cooper, R. Fu, S. H. Eichhorn and R. W. Schurko, *J. Am. Chem. Soc.*, 2008, **130**, 11056–11065.
- 40 M. P. Hildebrand, H. Hamaed, A. M. Namespetra, J. M. Donohue, R. Fu, I. Hung, Z. Gan and R. W. Schurko, *CrystEngComm*, 2014, **16**, 7334–7356.
- 41 M. K. Pandey, H. Kato, Y. Ishii, Y. Nishiyama, M. K. Pandey, H. Kato, Y. Ishii and Y. Nishiyama, *Phys. Chem. Chem. Phys.*, 2016, **18**, 6209–6216.
- 42 F. G. Vogt, *Solid-State NMR in Drug Discovery and Development*, 2013.
- 43 G. A. Monti, A. K. Chattah and Y. G. Linck, *Solid-State Nuclear Magnetic Resonance in Pharmaceutical Compounds*, Elsevier Ltd., 1st edn., 2014, vol. 83.
- 44 F. G. Vogt, *eMagRes*, 2015, **4**, 255–268.

- 45 D. C. Bradley, S. R. Hodge, J. D. Runnacles, M. Hughes, J. Mason and R. L. Richards, *J. Chem. Soc. Dalt. Trans.*, 1992, 1663.
- 46 G. S. Harbison, Y.-S. Kye, G. H. Penner, H. M. Grandin and M. Monette, *J. Phys. Chem. B*, 2002, **106**, 10285–10291.
- 47 T. N. Rudakov, V. T. Mikhaltsevitch, P. A. Hayes and W. P. Chisholm, *Chem. Phys. Lett.*, 2004, **387**, 405–409.
- 48 H. J. Jakobsen, A. R. Hove, R. G. Hazell, H. Bildsøe and J. Skibsted, *Magn. Reson. Chem.*, 2006, **44**, 348–356.
- 49 D. K. Lee, J. S. Santos and A. Ramamoorthy, *Chem. Phys. Lett.*, 1999, **309**, 209–214.
- 50 A. Portieri, R. K. Harris, R. A. Fletton, R. W. Lancaster and T. L. Threlfall, *Magn. Reson. Chem.*, 2004, **42**, 313–320.
- 51 T. Fujiwara, Y. Todokoro, H. Yanagishita and M. Tawarayama, *J. Biomol. NMR*, 2004, **28**, 311–325.
- 52 J.-P. Amoureux, J. Trébosc, B. Hu, N. Halpern-Manners and S. Antonijevic, *J. Magn. Reson.*, 2008, **194**, 317–320.
- 53 S. Antonijevic and N. Halpern-Manners, *Solid State Nucl. Magn. Reson.*, 2008, **33**, 82–87.
- 54 S. M. Althaus, K. Mao, J. A. Stringer, T. Kobayashi and M. Pruski, *Solid State Nucl. Magn. Reson.*, 2014, **57-58**, 17–21.
- 55 M. Ashikawa, A. Shoji, T. Ozaki and I. Ando, *Macromolecules*, 1999, **32**, 2288–2292.
- 56 T. Giavani, H. Bildsøe, J. Skibsted and H. J. Jakobsen, *J. Magn. Reson.*, 2004, **166**, 262–272.
- 57 F. Elmi and N. L. Hadipour, *J. Phys. Chem. A*, 2005, **109**, 1729–1733.
- 58 L. A. O’Dell and R. W. Schurko, *Phys. Chem. Chem. Phys.*, 2009, **11**, 7069–7077.
- 59 L. A. O’Dell, R. W. Schurko, K. J. Harris, J. Autschbach and C. I. Ratcliffe, *J. Am. Chem. Soc.*, 2011, **133**, 527–546.
- 60 L. A. O’Dell, C. I. Ratcliffe, X. Kong and G. Wu, *J. Phys. Chem. A*, 2012, **116**, 1008–14.
- 61 M. M. Elmi, A. A. Kaykhaei and F. Elmi, *Magn. Reson. Chem.*, 2012, **50**, 314–319.
- 62 S. L. Veinberg, Z. W. Friedl, K. J. Harris, L. A. O’Dell and R. W. Schurko, *CrystEngComm*, 2015, 17–19.
- 63 A. S. Tatton, T. N. Pham, F. G. Vogt, D. Iuga, A. J. Edwards and S. P. Brown, *CrystEngComm*, 2012, **14**, 2654.
- 64 A. S. Tatton, T. N. Pham, F. G. Vogt, D. Iuga, A. J. Edwards and S. P. Brown, *Mol. Pharm.*, 2013, **10**, 999–1007.
- 65 A. J. Rossini, L. Emsley and L. A. O’Dell, *Phys. Chem. Chem. Phys.*, 2014, **16**, 12890–12899.
- 66 K. J. Harris, S. L. Veinberg, C. R. Mireault, A. Lupulescu, L. Frydman and R. W. Schurko, *Chem. Eur. J.*, 2013, **19**, 16469–16475.
- 67 A. K. Chattah, R. Zhang, K. H. Mroue, L. Y. Pfund, M. R. Longhi, A. Ramamoorthy and

- C. Garnero, *Mol. Pharm.*, 2015, **12**, 731–741.
- 68 J. R. Smith, W. Xu and D. Raftery, *J. Phys. Chem. B*, 2006, **110**, 7766–76.
- 69 Y. Song, X. Yang, X. Chen, H. Nie, S. Byrn and J. W. Lubach, *Mol. Pharm.*, 2015, **12**, 857–866.
- 70 E. Balchin, D. J. Malcolm-Lawes, I. J. F. Poplett, M. D. Rowe, J. A. S. Smith, G. E. S. Pearce and S. A. C. Wren, *Anal. Chem.*, 2005, **77**, 3925–3930.
- 71 J. Barras, D. Murnane, K. Althoefer, S. Assi, M. D. Rowe, I. J. F. Poplett, G. Kyriakidou and J. A. S. Smith, *Anal. Chem.*, 2013, **85**, 2746–2753.
- 72 Z. Lavrič, J. Pirnat, J. Lužnik, J. Seliger, V. Žagar, Z. Trontelj and S. Srčič, *J. Pharm. Sci.*, 2010, **99**, 4857–4865.
- 73 J. Shinohara, K. Kobayashi, H. Sato-Akaba and H. Itozaki, *Solid State Nucl. Magn. Reson.*, 2011, **40**, 121–125.
- 74 A. Gregorovič and T. Apih, *J. Magn. Reson.*, 2013, **233**, 96–102.
- 75 J. N. Latosińska, M. Latosińska, J. Seliger, V. Žagar and Z. Kazimierczuk, *J. Phys. Chem. B*, 2014, **118**, 10837–10853.
- 76 L. A. O'Dell, *Prog. Nucl. Magn. Reson. Spectrosc.*, 2011, **59**, 295–318.
- 77 A. R. Hove, H. Bildsøe, J. Skibsted, M. Brorson and H. J. Jakobsen, *Inorg. Chem.*, 2006, **45**, 10873–81.
- 78 B. A. Whitehouse, J. D. Ray and D. J. Royer, *J. Magn. Reson.*, 1969, **1**, 311–326.
- 79 H. J. Jakobsen, A. R. Hove, H. Bildsøe, J. Skibsted and M. Brorson, *J. Magn. Reson.*, 2007, **185**, 159–163.
- 80 R. Tycko and S. J. Opella, *J. Chem. Phys.*, 1987, **86**, 1761–1774.
- 81 L. A. O'Dell and C. I. Ratcliffe, *Chem. Phys. Lett.*, 2011, **514**, 168–173.
- 82 L. A. O'Dell and A. Brinkmann, *J. Chem. Phys.*, 2013, **138**, 064201–10.
- 83 Y. Nishiyama, M. Malon, Z. Gan, Y. Endo and T. Nemoto, *J. Magn. Reson.*, 2013, **230**, 160–164.
- 84 V. Vitzthum, M. A. Caporini and G. Bodenhausen, *J. Magn. Reson.*, 2010, **205**, 177–179.
- 85 S. Cavadini, S. Antonijevic, A. Lupulescu and G. Bodenhausen, *J. Magn. Reson.*, 2006, **182**, 168–172.
- 86 S. Cavadini, S. Antonijevic, A. Lupulescu and G. Bodenhausen, *ChemPhysChem*, 2007, **8**, 1363–1374.
- 87 S. Cavadini, V. Vitzthum, S. Ulzega, A. Abraham and G. Bodenhausen, *J. Magn. Reson.*, 2010, **202**, 57–63.
- 88 S. Ulzega, *Chimia (Aarau)*, 2010, **64**, 157–160.
- 89 Z. Gan, J.-P. Amoureux and J. Trébosc, *Chem. Phys. Lett.*, 2007, **435**, 163–169.
- 90 S. Cavadini, *Prog. Nucl. Magn. Reson. Spectrosc.*, 2010, **56**, 46–77.
- 91 L. A. O'Dell and R. W. Schurko, *Chem. Phys. Lett.*, 2008, **464**, 97–102.

- 92 L. A. O'Dell, A. J. Rossini and R. W. Schurko, *Chem. Phys. Lett.*, 2009, **468**, 330–335.
- 93 L. A. O'Dell and R. W. Schurko, *J. Am. Chem. Soc.*, 2009, **131**, 6658–6659.
- 94 L. A. O'Dell and C. I. Ratcliffe, *Chem. Commun.*, 2010, **46**, 6774–6776.
- 95 Ě. Kupĉe and R. Freeman, *J. Magn. Reson. Ser. A*, 1995, **115**, 273–276.
- 96 R. Bhattacharyya and L. Frydman, *J. Chem. Phys.*, 2007, **127**, 1–8.
- 97 S. E. Shore, J.-P. Ansermet, C. P. Slichter and J. H. Sinfelt, *Phys. Rev. Lett.*, 1987, **58**, 953–956.
- 98 D. Massiot, I. Farnan, N. Gautier, D. Trumeau, A. Trokiner and J. P. Coutures, *Solid State Nucl. Magn. Reson.*, 1995, **4**, 241–248.
- 99 A. Medek, V. Frydman and L. Frydman, *J. Phys. Chem. A*, 1999, **103**, 4830–4835.
- 100 A. W. MacGregor, L. A. O'Dell and R. W. Schurko, *J. Magn. Reson.*, 2011, **208**, 103–113.
- 101 B. E. G. Lucier, A. R. Reidel and R. W. Schurko, *Can. J. Chem.*, 2011, **89**, 919–937.
- 102 B. E. G. Lucier, K. E. Johnston, W. Xu, J. C. Hanson, S. D. Senanayake, S. Yao, M. W. Bourassa, M. Srebro, J. Autschbach and R. W. Schurko, *J. Am. Chem. Soc.*, 2014, **136**, 1333–1351.
- 103 J. Xu, B. E. G. Lucier, Z. Lin, A. Sutrisno, V. V Terskikh and Y. Huang, *J. Phys. Chem. C*, 2014, **118**, 27353–27365.
- 104 K. E. Johnston, C. A. O'Keefe, R. M. Gauvin, J. Trébosc, L. Delevoye, J.-P. Amoureux, N. Popoff, M. Taoufik, K. Oudatchin and R. W. Schurko, *Chem. Eur. J.*, 2013, **19**, 12396–12414.
- 105 C. A. O'Keefe, K. E. Johnston, K. Sutter, J. Autschbach, R. M. Gauvin, J. Trebosc, L. Delevoye, N. Popoff, M. Taoufik, K. A. Udachin and R. W. Schurko, *Inorg. Chem.*, 2014, **53**, 9581–9597.
- 106 J. Viger-Gravel, I. Korobkov and D. L. Bryce, *Cryst. Growth Des.*, 2011, **11**, 4984–4995.
- 107 A. Faucher, V. V Terskikh and R. E. Wasylshen, *Solid State Nucl. Magn. Reson.*, 2014, **61-62**, 54–61.
- 108 H. Yu, X. Tan, G. M. Bernard, V. V Terskikh, J. Chen and R. E. Wasylshen, *J. Phys. Chem. A*, 2015, **119**, 8279–8293.
- 109 K. J. Harris, A. Lupulescu, B. E. G. Lucier, L. Frydman and R. W. Schurko, *J. Magn. Reson.*, 2012, **224**, 38–47.
- 110 Y. Ishii and R. Tycko, *J. Magn. Reson.*, 2000, **142**, 199–204.
- 111 Y. Ishii, J. P. Yesinowski and R. Tycko, *J. Am. Chem. Soc.*, 2001, **123**, 2921–2922.
- 112 K. Mao, J. W. Wiench, V. S.-Y. Lin and M. Pruski, *J. Magn. Reson.*, 2009, **196**, 92–95.
- 113 E. K. Paulson, C. R. Morcombe, V. Gaponenko, B. Dancheck, R. A. Byrd and K. W. Zilm, *J. Am. Chem. Soc.*, 2003, **125**, 15831–15836.
- 114 T. Pawlak, P. Paluch, K. Trzeciak-Karlikowska, A. Jeziorna and M. J. Potrzebowski, *CrystEngComm*, 2013, **15**, 8680–8692.

- 115 J. W. Wiench, C. E. Bronnimann, V. S.-Y. Lin and M. Pruski, *J. Am. Chem. Soc.*, 2007, **129**, 12076–12077.
- 116 T. Kobayashi, K. Mao, S. G. Wang, V. S.-Y. Lin and M. Pruski, *Solid State Nucl. Magn. Reson.*, 2011, **39**, 65–71.
- 117 S. Hediger, B. H. Meier and R. R. Ernst, *Chem. Phys. Lett.*, 1995, **240**, 449–456.
- 118 K. Mao and M. Pruski, *J. Magn. Reson.*, 2009, **201**, 165–174.
- 119 A. W. Overhauser, *Phys. Rev.*, 1953, **92**, 411–415.
- 120 T. R. Carver and C. P. Slichter, *Phys. Rev.*, 1953, **92**, 212–213.
- 121 C. D. Joye, R. G. Griffin, M. K. Hornstein, K. Hu, K. E. Kreisler, M. Rosay, M. A. Shapiro, J. R. Sirigiri, R. J. Temkin and P. P. Woskov, *IEEE Trans. Plasma Sci.*, 2006, **34**, 518–523.
- 122 A. B. Barnes, M. L. Mak-jurkauskas, Y. Matsuki, V. S. Bajaj, P. C. A. Van Der Wel, R. Derocher, J. Bryant, J. R. Sirigiri, R. J. Temkin, J. Lugtenburg, J. Herzfeld and R. G. Griffin, *J. Magn. Reson.*, 2009, **198**, 261–270.
- 123 C. Song, K. Hu, C. Joo, T. M. Swager and R. G. Griffin, *J. Am. Chem. Soc.*, 2006, **128**, 11385–11390.
- 124 A. Zagdoun, G. Casano, O. Ouari, M. S. Der, A. J. Rossini, F. Aussenac, M. Yulikov, G. Jeschke, C. Cope, A. Lesage, P. Tordo and L. Emsley, *J. Am. Chem. Soc.*, 2013, **135**, 12790–12797.
- 125 T. Maly, G. T. Debelouchina, V. S. Bajaj, K. Hu, C. Joo, M. L. M. Jurkauskas, J. R. Sirigiri, P. C. A. Van Der Wel, J. Herzfeld, R. J. Temkin and R. G. Griffin, *J. Chem. Phys.*, 2008, **128**, 052211–19.
- 126 A. Lesage, M. Lelli, D. Gajan, M. A. Caporini, V. Vitzthum, P. Mie, J. Alauzun, A. Roussey, A. Mehdi and G. Bodenhausen, *J. Am. Chem. Soc.*, 2010, **132**, 15459–15461.
- 127 H. Takahashi, D. Lee, L. Dubois, M. Bardet, S. Hediger and G. De Paëpe, *Angew. Chemie Int. Ed.*, 2012, **51**, 11766–11769.
- 128 F. A. Perras, T. Kobayashi and M. Pruski, *J. Am. Chem. Soc.*, 2015, **137**, 8336–8339.
- 129 A. Zagdoun, G. Casano, O. Ouari, G. Lapadula, A. J. Rossini, M. Lelli, M. Baffert, D. Gajan, L. Veyre, W. E. Maas, M. Rosay, R. T. Weber, C. Thieuleux, C. Coperet, A. Lesage, P. Tordo and L. Emsley, *J. Am. Chem. Soc.*, 2012, **134**, 2284–2291.
- 130 Z. Guo, T. Kobayashi, L. Wang, W. Goh, C. Xiao, M. A. Caporini, M. Rosay, D. D. Johnson, M. Pruski and W. Huang, *Chem. Eur. J.*, 2014, 16308–16313.
- 131 T. Kobayashi, S. Gupta, M. A. Caporini, V. K. Pecharsky and M. Pruski, *J. Phys. Chem. C*, 2014, **118**, 19548–19555.
- 132 I. Csöreg, *Acta Crystallogr. Sect. C Cryst. Struct. Commun.*, 1992, **48**, 1794–1798.
- 133 G. Nolze and W. Kraus, *Powder Diffr.*, 1998, **13**, 256–259.
- 134 R. Glaser, D. Shiftan and M. Drouin, *Can. J. Chem.*, 2000, **78**, 212–223.
- 135 Y. Barrans, M. Cotrait and J. Dangoumau, *Acta Crystallogr. Sect. B Struct. Crystallogr. Cryst. Chem.*, 1973, **29**, 1264–1272.

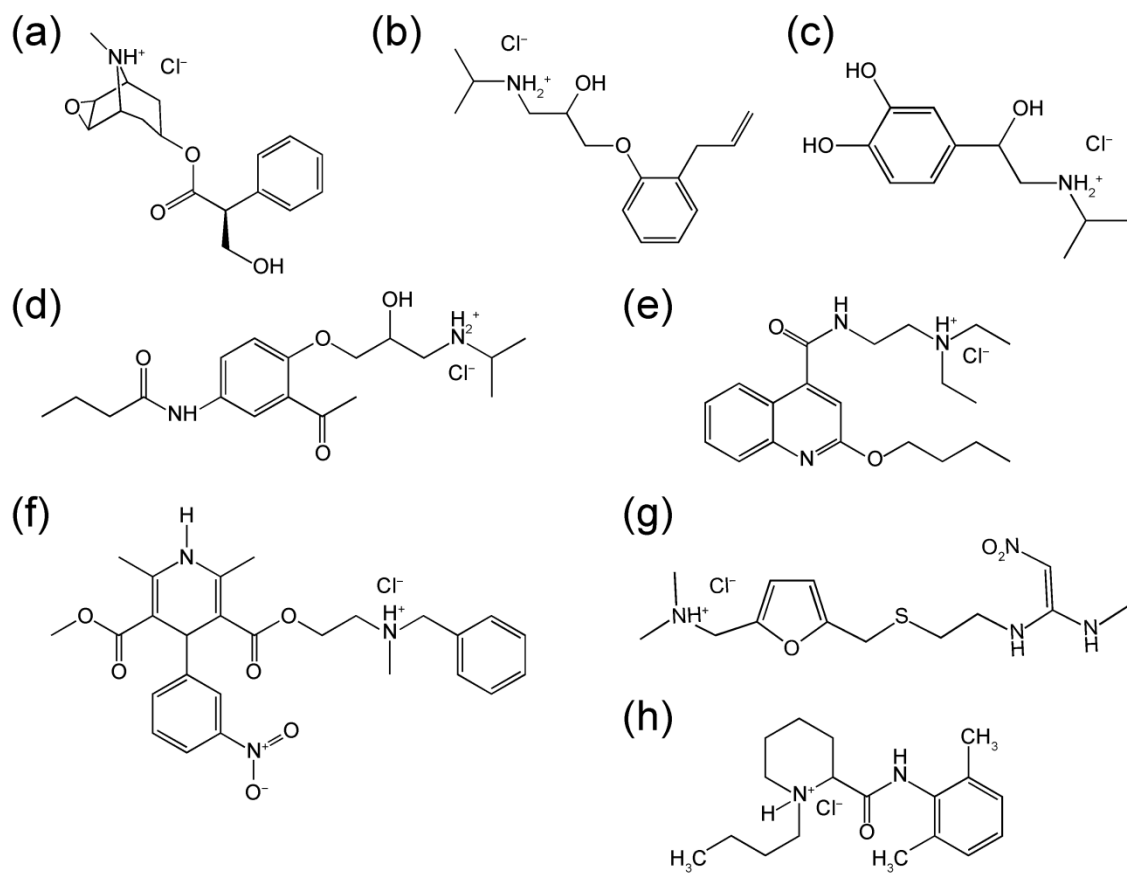
- 136 R. Kingsford-Adaboh, E. Hayashi, M. Haisa and S. Kashida, *Bull. Chem. Soc. Jpn.*, 1993, **66**, 2883–2888.
- 137 A. Carpy, M. Gadret, D. Hickel and J. M. Leger, *Acta Cryst. B.*, 1979, **35**, 185–188.
- 138 B. S. Hayward and J. Donohue, *J. Cryst. Mol. Struct.*, 1977, **7**, 275–294.
- 139 E. Moreno-Calvo, M. Muntó, K. Wurst, N. Ventosa, N. Masciocchi and J. Veciana, *Mol. Pharm.*, 2011, **8**, 395–404.
- 140 T. Ishida, Y. In and M. Inoue, *Acta Crystallogr. Sect. C Cryst. Struct. Commun.*, 1990, **46**, 1893–1896.
- 141 J. A. Tang, J. D. Masuda, T. J. Boyle and R. W. Schurko, *ChemPhysChem*, 2006, **7**, 117–130.
- 142 K. Eichele, 2013.
- 143 B. M. Fung, A. K. Khitrin and K. Ermolaev, *J. Magn. Reson.*, 2000, **142**, 97–101.
- 144 T. G. Oas, R. G. Griffin and M. H. Levitt, *J. Chem. Phys.*, 1988, **89**, 692–695.
- 145 V. E. Zorin, 2013.
- 146 R. K. Harris, E. D. Becker, S. M. C. De Menezes, P. Granger, R. E. Hoffman and K. W. Zilm, *Pure Appl. Chem.*, 2008, **80**, 59–84.
- 147 S. J. Clark, M. D. Segall, C. J. Pickard, P. J. Hasnip, M. I. J. Probert, K. Refson and M. C. Payne, *Zeitschrift für Krist.*, 2005, **220**, 567–570.
- 148 C. J. Pickard and F. Mauri, *Phys. Rev. B*, 2001, **63**, 245101–13.
- 149 R. K. Harris and A. C. Olivieri, *Prog. Nucl. Magn. Reson. Spectrosc.*, 1992, **24**, 435–456.
- 150 S. K. Amini, H. Shaghghi, A. D. Bain, A. Chabok and M. Tafazzoli, *Solid State Nucl. Magn. Reson.*, 2010, **37**, 13–20.
- 151 J. G. Hexem, M. H. Frey and S. J. Opella, *J. Am. Ceram. Soc.*, 1981, **103**, 224–226.
- 152 A. P. Cox, S. Waring and K. Motgenstern, *Nature*, 1971, **229**, 22–23.
- 153 A. P. Cox and S. Waring, *J. Chem. Soc. Faraday Trans. 2*, 1972, **6**, 1060–1071.
- 154 S. N. Subbarao and P. J. Bray, *J. Chem. Phys.*, 1977, **67**, 3947–3955.
- 155 R. K. Harris, P. Jonsen and K. J. Packer, *Magn. Reson. Chem.*, 1985, **23**, 565–577.
- 156 T. Kobayashi, K. Mao, P. Paluch, A. Nowak-Kröl, J. Sniechowska, Y. Nishiyama, D. T. Gryko, M. J. Potrzebowski and M. Pruski, *Angew. Chemie - Int. Ed.*, 2013, **52**, 14108–14111.
- 157 Y. Qi, M. Malon, C. Martineau, F. Taulelle and Y. Nishiyama, *J. Magn. Reson.*, 2014, **239**, 75–80.
- 158 Y. Nishiyama, T. Kobayashi, M. Malon, D. Singappuli-Arachchige, I. I. Slowing and M. Pruski, *Solid State Nucl. Magn. Reson.*, 2015, **66**, 56–61.
- 159 E. R. McNellis, J. Meyer and K. Reuter, *Phys. Rev. B - Condens. Matter Mater. Phys.*, 2009, **80**, 1–10.
- 160 R. K. Harris, R. E. Wasylshen and M. J. Duer, Eds., *NMR Crystallography*, John Wiley & Sons, Ltd., Chichester, U.K., 2009.

- 161 M. Baias, C. M. Widdifield, J.-N. Dumez, H. P. G. Thompson, T. G. Cooper, E. Salager, S. Bassil, R. S. Stein, A. Lesage, G. M. Day and L. Emsley, *Phys. Chem. Chem. Phys.*, 2013, **15**, 8069–80.
- 162 B. D. Malone and M. L. Cohen, *Phys. Rev. B - Condens. Matter Mater. Phys.*, 2012, **85**, 1–5.
- 163 A. J. Morris, C. P. Grey, R. J. Needs and C. J. Pickard, *Phys. Rev. B*, 2011, **84**, 224106.
- 164 C. J. Pickard and R. J. Needs, *J. Phys. Condens. Matter*, 2011, **23**, 053201.
- 165 M. Dračinský and P. Hodgkinson, *CrystEngComm*, 2013, **15**, 8705–8712.
- 166 G. Rossi and R. Ferrando, *J. Phys. Condens. Matter*, 2009, **21**, 084208.
- 167 J. C. Schön, K. Doll and M. Jansen, *Phys. Status Solidi Basic Res.*, 2010, **247**, 23–39.

Table 1: Experimental^a and calculated^b (using CASTEP) ¹⁴N EFG tensor and nitrogen chemical shift parameters.

API	Site	Expt. C _Q (MHz) ^c	Calc. C _Q (MHz)	Expt. η _Q ^d	Calc. η _Q	Expt. δ _{iso} (ppm)	Calc. σ _{iso} (ppm) ⁱ
Scop ^e	RR'R''NH ⁺	1.29(5)	-1.36	0.29(3)	0.37	-332(1)	169.04
Alpr ^f	RR'NH ₂ ⁺	1.13(3)	1.53	0.82(3)	0.63	-346(2)	154.45
Isop ^f	RR'NH ₂ ⁺	1.01(2)	1.08	0.91(3)	0.85	-345(1)	168.36
Aceb ^f	RR'NH ₂ ⁺	1.04(3)	-1.10	0.90(2)	0.86	-329(1) ^h	156.40
	RR'NH	-	-3.39	-	0.40	-250(1)	85.30
Dibu	RR'R''NH ⁺	-	-1.51	-	0.17	-326(2)	165.27
	RR'NH	-	-3.48	-	0.33	-264(1)	97.17
	RR'N	-	-3.99	-	0.07	-135(3) ^g	-32.67
Nica ^f	RR'R''NH ⁺	1.43(3)	-1.31	0.14(2)	0.24	-348(2)	170.32
	RR'NH	-	-2.97	-	0.33	-265(5)	74.99
	RNO ₂	-	-1.10	-	0.20	-	-144.25
Rani ^f	RR'R''NH ⁺	1.62(10)	-1.50	0.22(5)	0.17	-340(2)	176.40
	RR'NH	3.25(10)	-3.82	0.50(5)	0.38	-281(2)	143.70
	RR'NH	3.25(10)	-3.68	0.58(5)	0.53	-292(2)	133.25
	RNO ₂	1.15(5)	1.32	0.49(5)	0.37	-22(2)	-113.27
Bupi ^f	RR'R''NH ⁺	1.00(3)	-1.16	0.30(3)	0.29	-342(1)	162.27
	RR'NH	-	-3.20	-	0.40	-269(1)	89.77
Bupi II ^f	RR'R''NH ⁺	1.25 (4)	-1.54	0.19(4)	0.18	-345(2)	162.94
	RR'NH	-	-3.38	-	0.44	-267(2)	85.30

^aThe uncertainty in the last digit(s) of each value is denoted in brackets. ^bEFG and chemical shift parameters were calculated after optimization of the proton positions. ^cC_Q = eQV_{33}/h . ^dη_Q = (V₁₁ - V₂₂)/V₃₃. ^eSpectra acquired using DE. ^fSpectra acquired using BCP. ^gSite observed using a longer contact time (Figure S9). ^hSite observed using DNP-enhanced ¹⁵N{¹H} CP/MAS. ⁱ See SI for conversion procedure from calc. σ_{iso} to calc. δ_{iso}.



Scheme 1: Schematic representations of HCl salts of APIs studied by ¹⁴N and ¹⁵N SSNMR: (a) Scopolamine (**Scop**), (b) Alprenolol (**Alpr**), (c) Isoprenaline (**Isop**), (d) Acebutolol (**Aceb**), (e) Dibucaine (**Dibu**), (f) Nicardipine (**Nica**), (g) Ranitidine (**Rani**), and (h) Bupivacaine (**Bupi**).

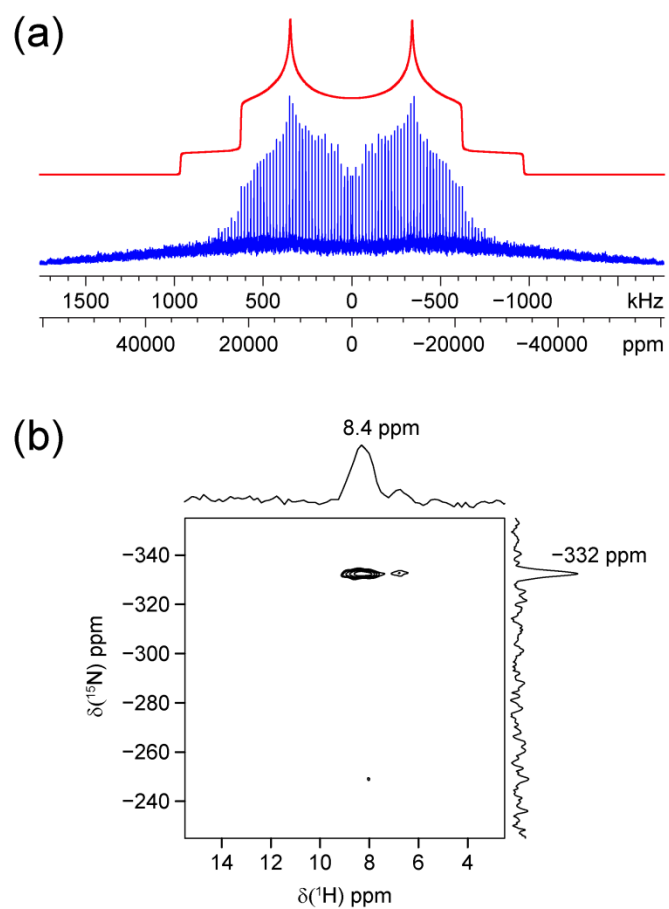


Figure 1: (a) Static ^{14}N SSNMR spectrum (9.4 T using DE) and (b) $^1\text{H}\{^{15}\text{N}\}$ idHETCOR spectrum (14.1 T) of **Scop**. We refer the reader to the Supporting Information, SI, for detailed lists of the acquisition parameters.

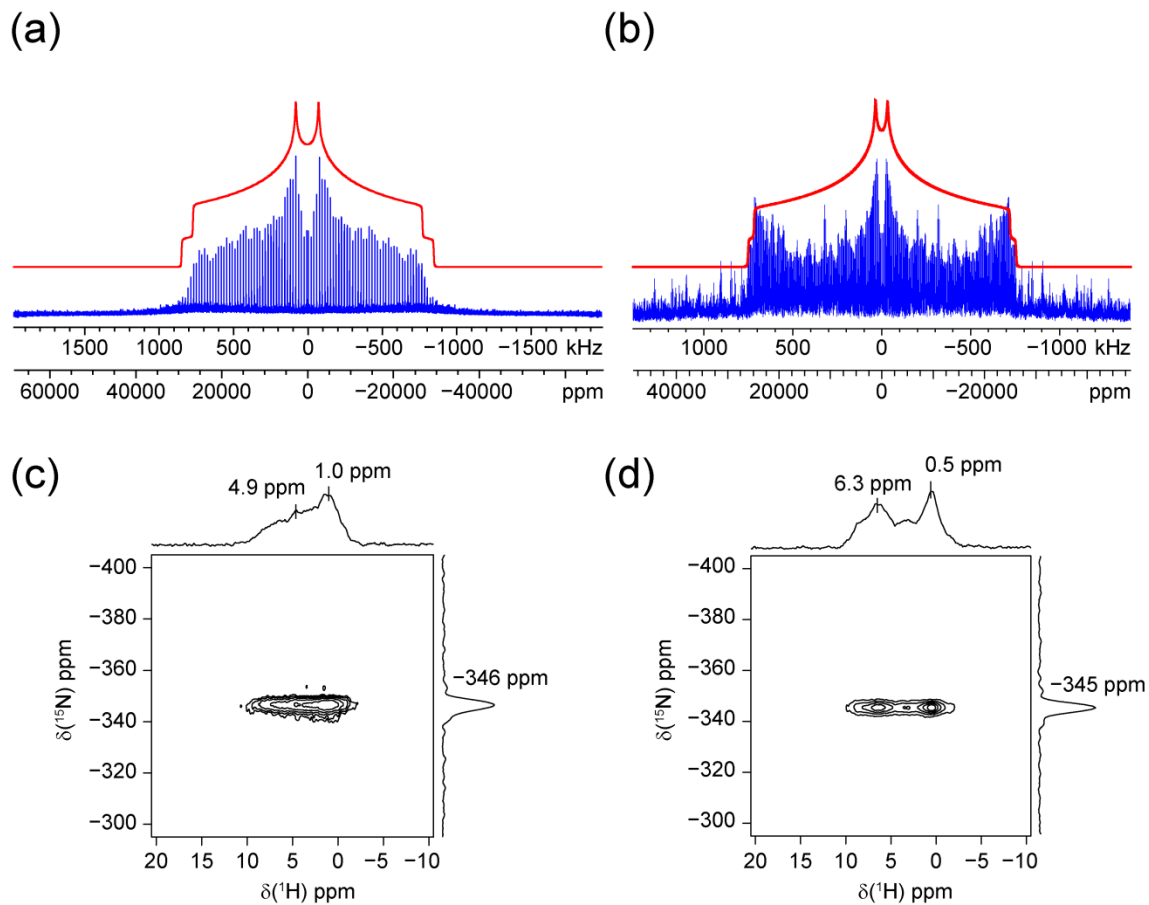


Figure 2: Static ^{14}N SSNMR spectra (9.4 T using BCP) of (a) **Alpr** and (b) **Isop**. $^1\text{H}\{^{15}\text{N}\}$ idHETCOR (14.1 T) spectra of (c) **Alpr** and (d) **Isop**.

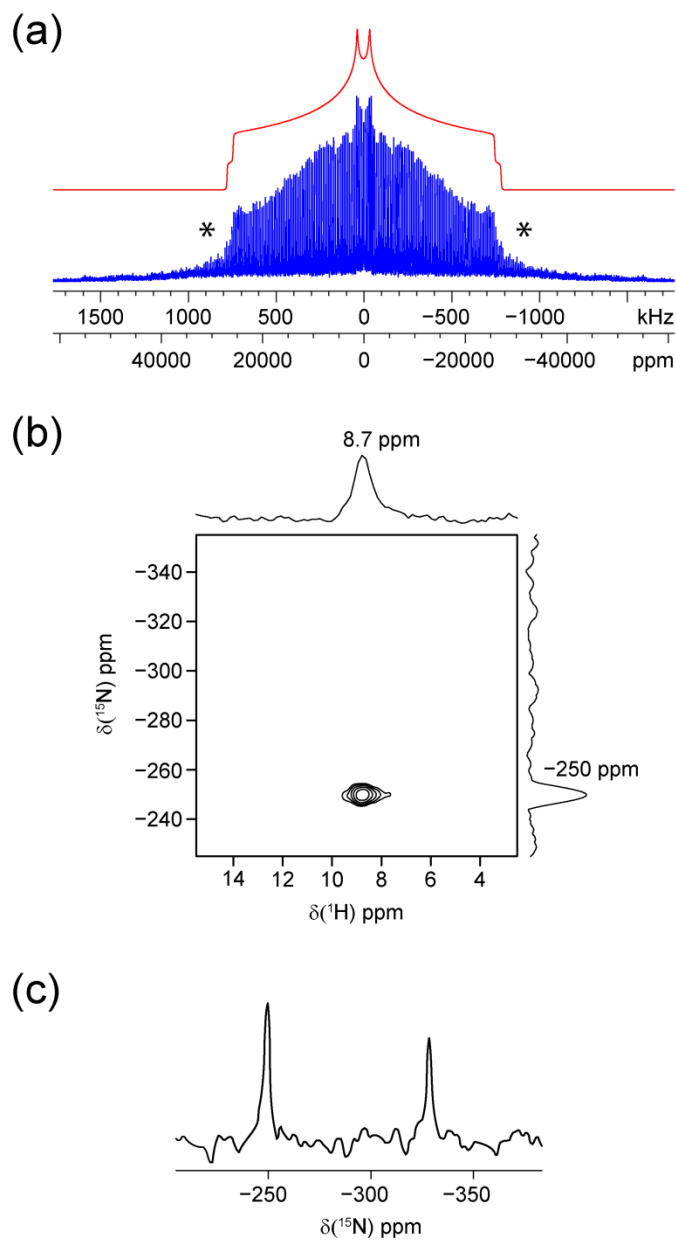


Figure 3: (a) Static ^{14}N SSNMR spectrum (9.4 T using BCP), (b) $^1\text{H}\{^{15}\text{N}\}$ idHETCOR spectrum (14.1 T), and (c) DNP-enhanced $^{15}\text{N}\{^1\text{H}\}$ CP/MAS spectrum (263 GHz gyrotron, 9.4 T magnet) of **Aceb**. In (a) signal corresponding to the RR'NH moiety is denoted by *.

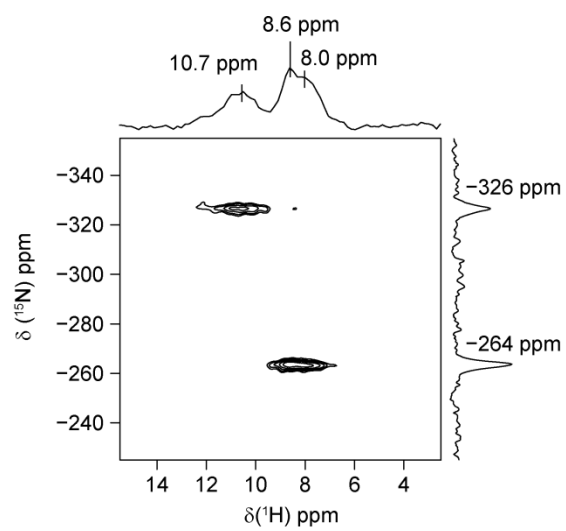


Figure 4: $^1\text{H}\{^{15}\text{N}\}$ idHETCOR spectrum (14.1 T) of **Dibu**.

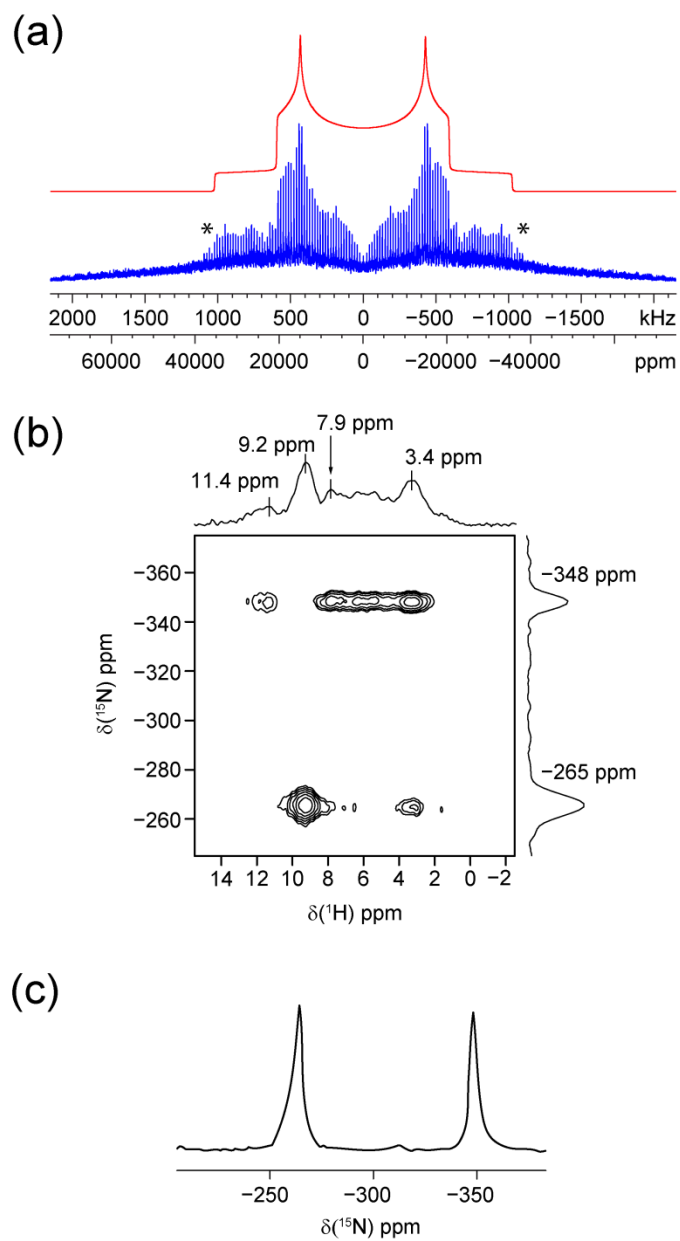


Figure 5: (a) Static ^{14}N SSNMR spectrum (9.4 T using BCP), (b) $^1\text{H}\{^{15}\text{N}\}$ idHETCOR spectrum (14.1 T), and (c) DNP-enhanced $^{15}\text{N}\{^1\text{H}\}$ CP/MAS spectrum (263 GHz gyrotron, 9.4 T magnet) of **Nica**. In (a) signal corresponding to one of the other nitrogen sites is observed, as denoted by *.

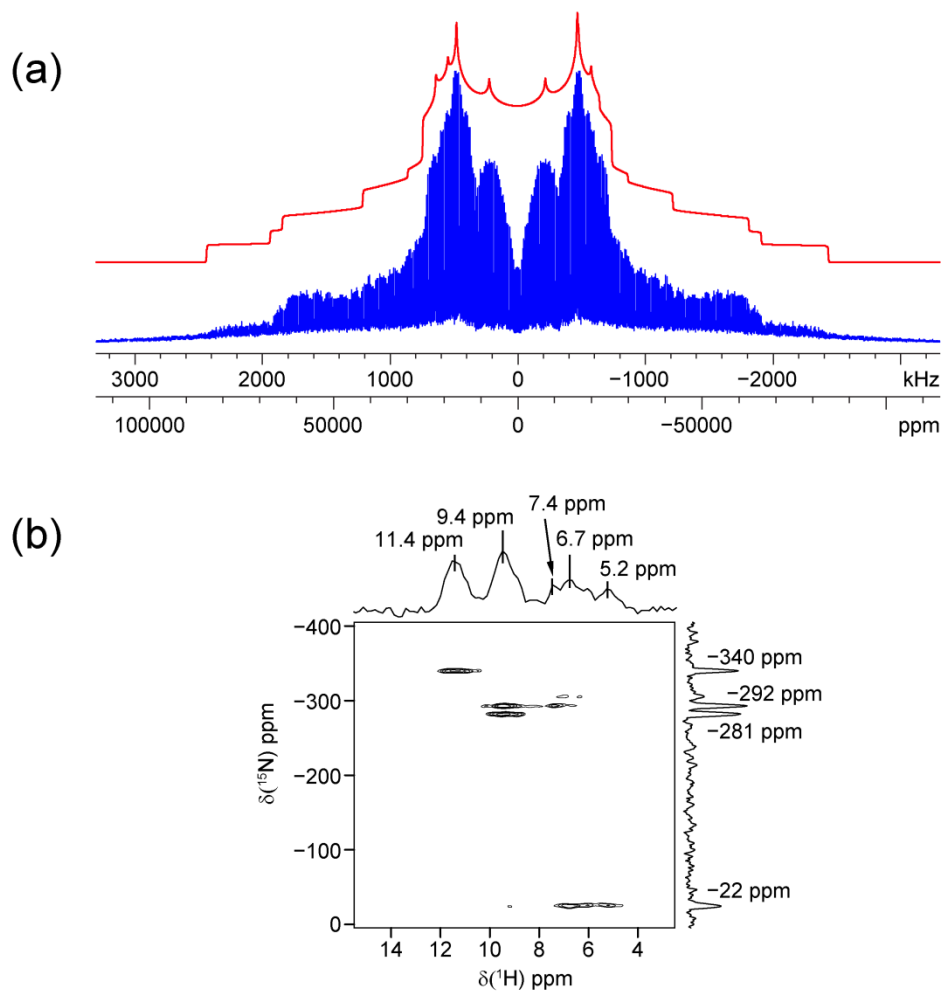


Figure 6: (a) Static ^{14}N SSNMR spectrum (9.4 T using BCP) and (b) $^1\text{H}\{^{15}\text{N}\}$ idHETCOR spectrum (14.1 T) of **Rani**.

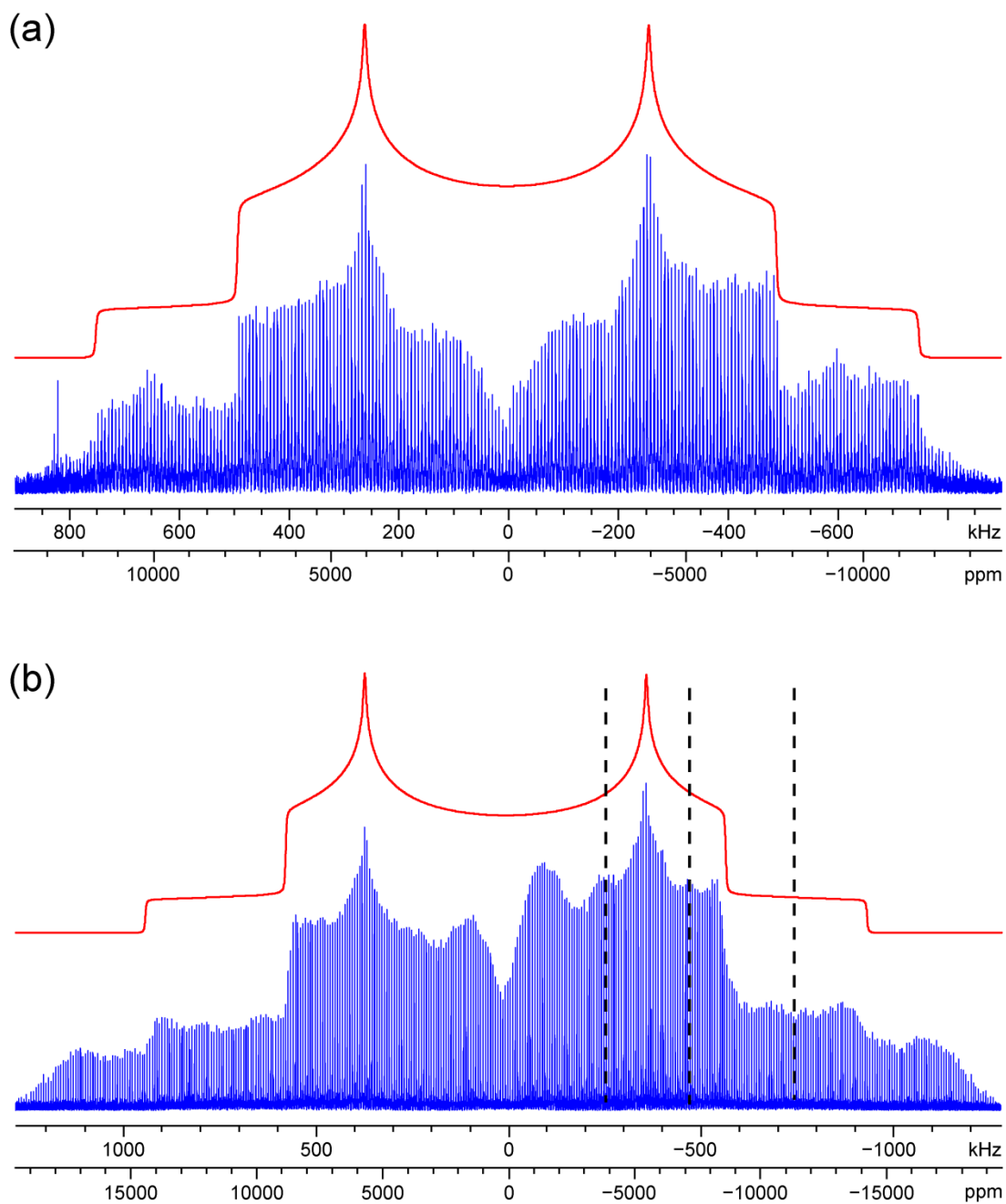


Figure 7: Static ^{14}N SSNMR spectra (21.1 T using DE) acquired for (a) **Bupi** and (b) **Bupi II**. The total powder pattern was acquired for each, i.e., no “mirroring” was performed. Dashed lines corresponding to the discontinuities of **Bupi** are also shown in (b) for comparison.

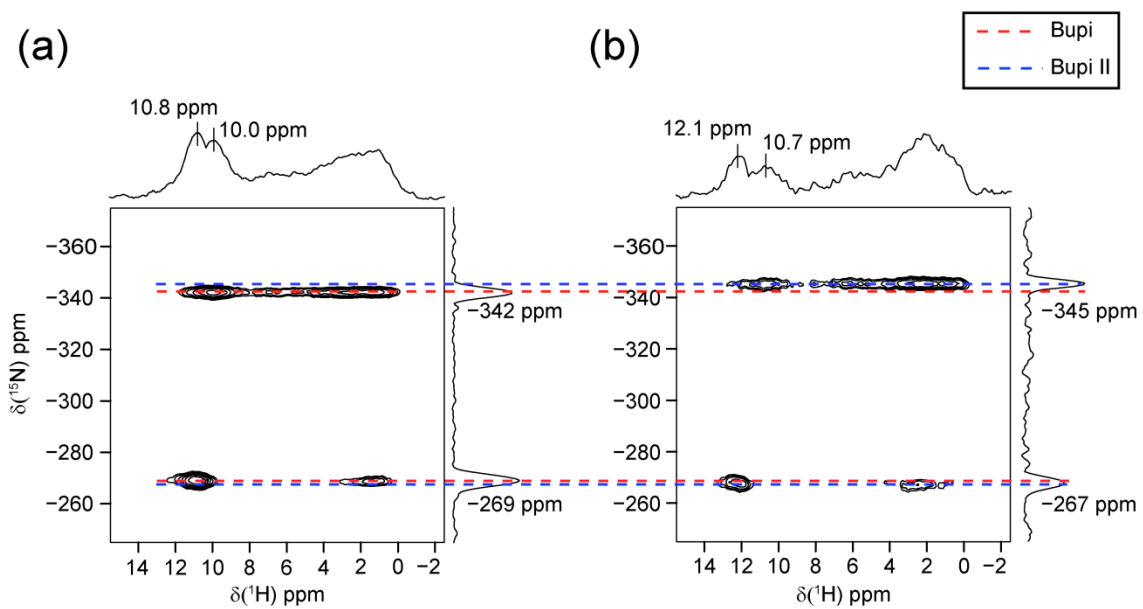


Figure 8: $^1\text{H}\{^{15}\text{N}\}$ idHETCOR spectra (14.1 T) of (a) **Bupi** and (b) **Bupi II**.

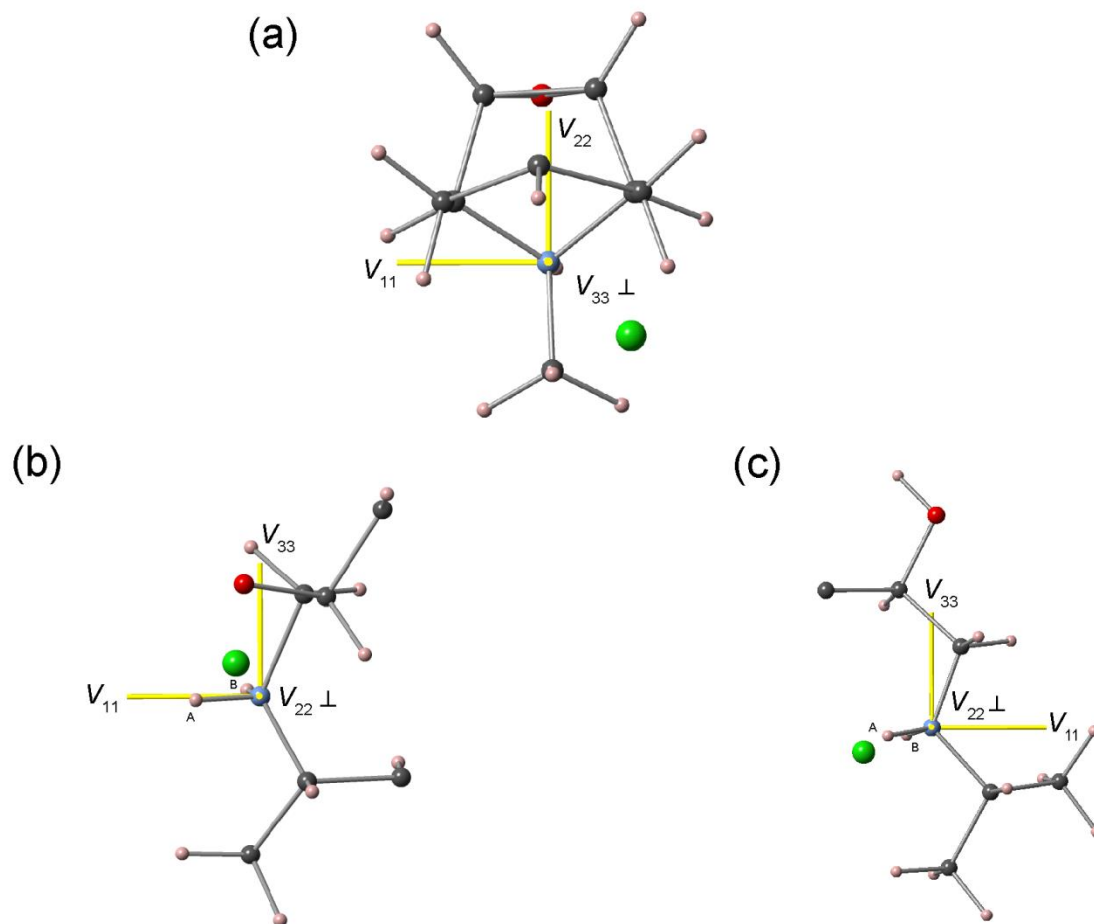


Figure 9: Theoretical ^{14}N EFG tensor orientations in the molecular frames of (a) **Scop**, (b) **Alpr**, and (c) **Isop**. Tensor orientations are taken from ^{14}N EFG calculations completed using NMR CASTEP after geometry optimization of the proton positions. Molecular fragments shown for clarity (see SI for full structures).

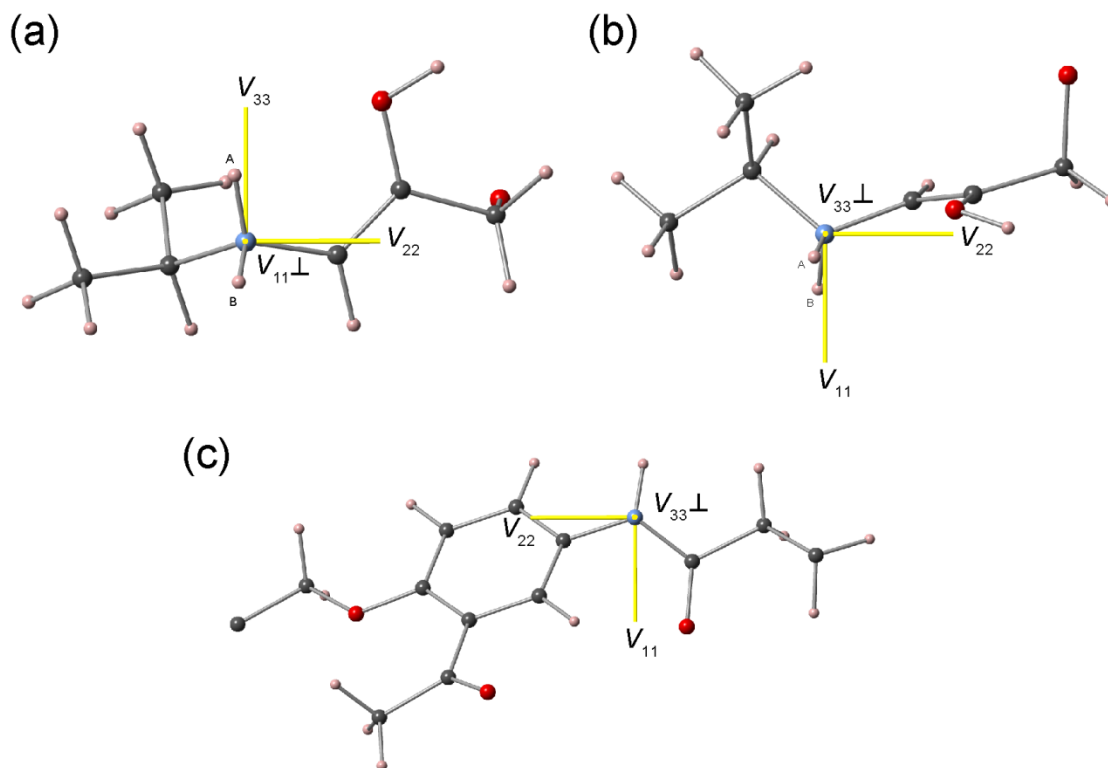


Figure 10: Theoretical ^{14}N EFG tensor orientations in the molecular frames of (a,b) the pseudo-tetrahedral nitrogen and (c) the planar nitrogen in **Aceb**. In (a) the molecular frame is viewed down the V_{11} component of the tensor and in (b) the molecule is viewed down V_{33} . Molecular fragments shown for clarity (see SI for full structure).

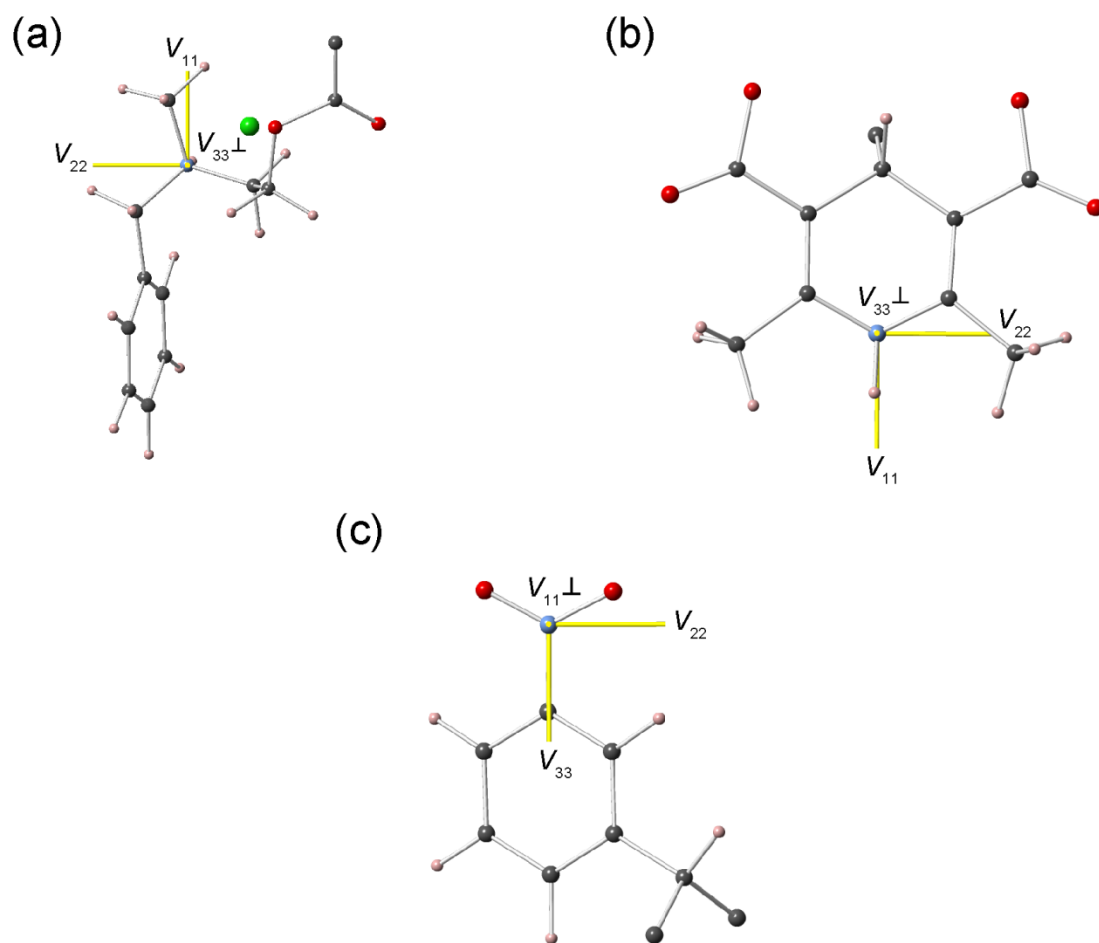


Figure 11: Theoretical ^{14}N EFG tensor orientations in the molecular frames of **Nica**. In (a) the pseudo-tetrahedral $RR'R''\text{NH}^+$ site, (b) the planar $RR'\text{NH}$ nitrogen, and (c) the RNO_2 group. Molecular fragments shown for clarity (see SI for full structure).

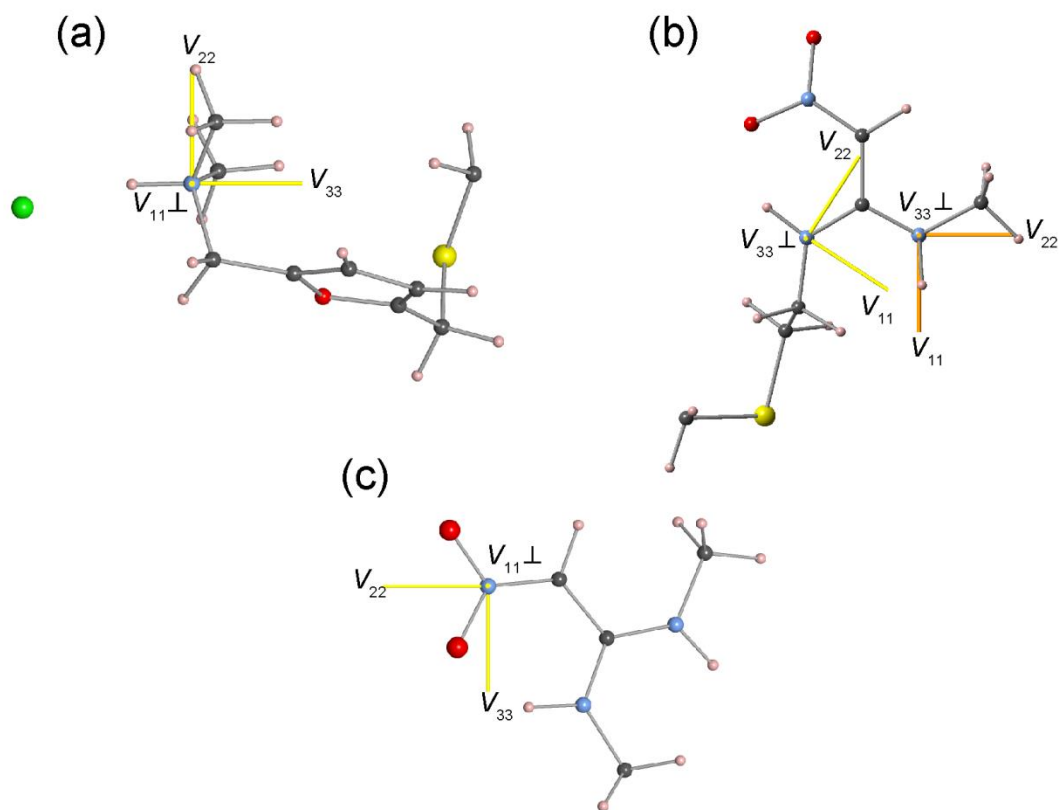


Figure 12: Theoretical ^{14}N EFG tensor orientations in the molecular frame of **Rani**. In (a) the pseudo-tetrahedral $\text{RR}'\text{R}''\text{NH}^+$ site, (b) the two planar $\text{RR}'\text{NH}$ nitrogen groups, and (c) the RNO_2 group. Molecular fragments are shown for clarity (see SI for full structure).

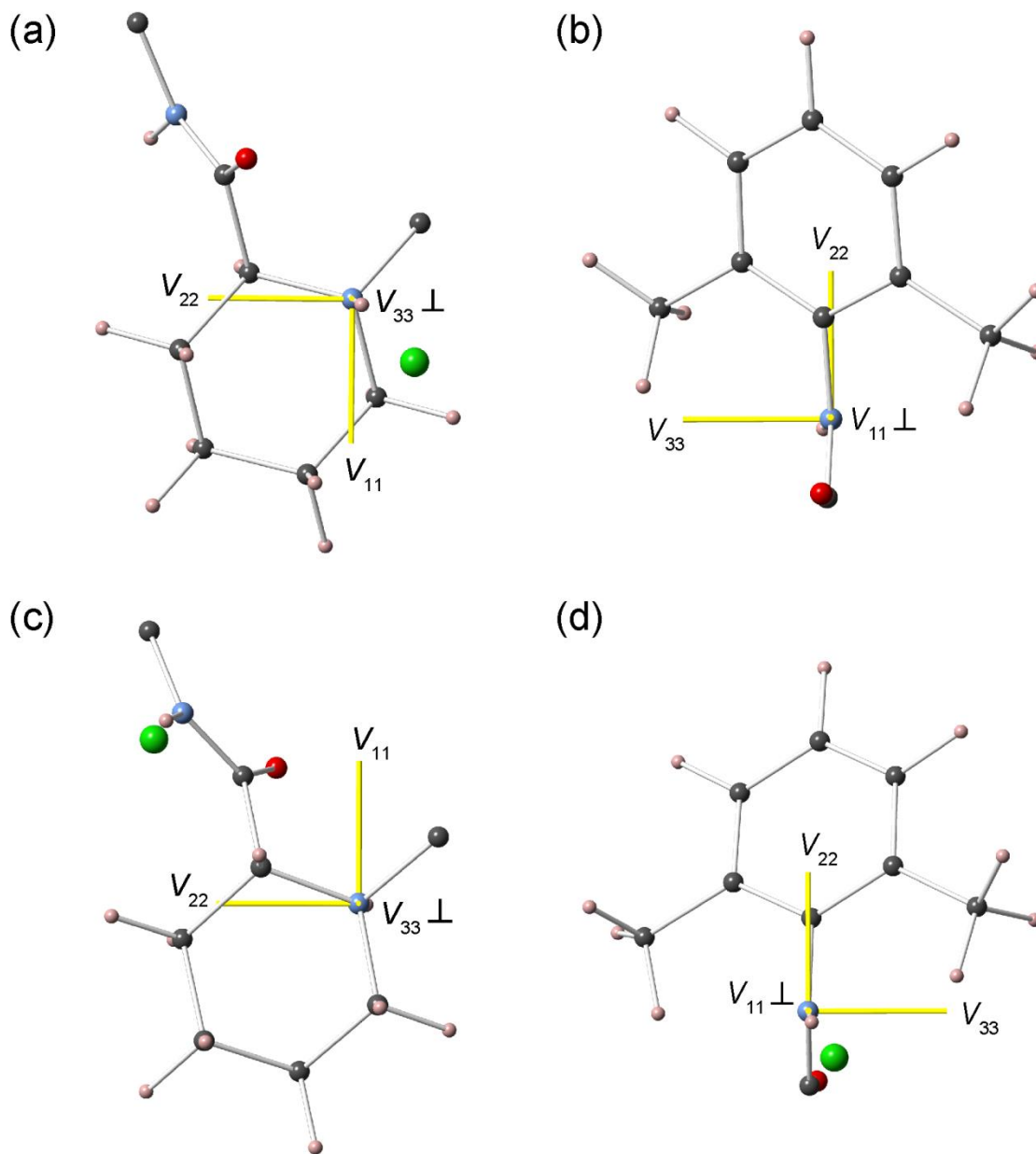


Figure 13: Theoretical ^{14}N EFG tensor orientations in the molecular frames of **Bupi** (a and b) and **Bupi II** (c and d). The ^{14}N EFG tensors of the pseudo-tetrahedral $\text{RR}'\text{R}''\text{NH}^+$ sites are depicted in (a) and (c), while the planar $\text{RR}'\text{NH}$ nitrogen groups are depicted in (b) and (d). Molecular fragments shown for clarity (see SI for full structures).